Photo- and electrochemical processes to convert plastic waste into fuels and high-value chemicals

Xinxin Liang, Ximing Li, Qibing Dong, Ting Gao, Mengxin Cao, Ke Zhao, Eric Lichtfouse, Antonio Otavio T Patrocinio, Chuanyi Wang

Chemical Engineering Journal 482 (2024) 148827

https://doi.org/10.1016/j.cej.2024.148827

Review

Photo- and electrochemical processes to convert plastic waste into fuels and high-value chemicals

Xinxin Liang [a], Ximing Li [a], Qibing Dong [a], Ting Gao [a], Mengxin Cao [a], Ke Zhao [a], Eric Lichtfouse [b], Antonio Otavio T. Patrocinio [c], Chuanyi Wang [a,*]

[a] School of Environmental Science and Engineering, Shaanxi University of Science and Technology, 710021 Xi'an PR China
[b] State Key Laboratory of Multiphase Flow in Power Engineering, Xi'an Jiaotong University, 710049 Xi'an Shaanxi PR China
[c] Laboratory of Photochemistry and Materials Science – LAFOT-CM, Universidade Federal de Uberlandia, 38400-902, Uberlandia, MG, Brazil

ARTICLE INFO

Keywords:
Electroreforming
H_2 evolution
Photoreforming
Plastic upcycling
Waste plastics

ABSTRACT

The massive waste of plastics is resulting in serious environmental issues, yet plastics can be regarded as raw carbon materials to produce value-added chemicals by catalytic methods. In particular, recently-developed photocatalytic and electrocatalytic processes are promising for plastic conversion. Recent reviews about plastic recycling focus on traditional thermochemical methods, however, there have been few reported reviews on advanced photo- and electrochemical processes. Therefore, here we review clean catalytic technologies to convert plastics into fuels, materials and fine chemicals, with focus on photo-, electro-, photoelectrochemical catalysis and solar thermal electrochemical processes. The catalytic mechanisms, processes, conditions as well as pretreatment methods for various plastics upcylcing are discussed and summarized, challenges are explained, and directions for upgrading and transforming plastics in the future are proposed.

1. Introduction

Since the phenolic resin was first synthesized in 1907, many types of plastics derived from fossil fuels have been widely applied in various fields of human production and life, because of their low cost, high stability, and processability [1,2]. More than 6000 Mt of plastic waste have been worldly produced from 1950 to 2015, and the annual production of plastic waste continues to increase at a rate of 4 % [3,4]. Plastic waste causes serious pollution issues [5,6]. For example, plastic waste in soils affect the absorption of water and nutrients by crops and lead to the reduction of the crop yield [7]. Moreover, nano- and microplastics can integrate ecological cycles from water to plants and animals, and thus end up in human bodies, damaging human health [8]. Therefore, plastics should be recycled as much as possible, yet plastic recycling is actually very challenging [9].

Actually, the main methods of plastic disposal are landfilling, incineration and secondary recycling (Fig. 1). Plastic landfilling is a simple and low-cost technology, but this method requires a large amount of land, changes the soil pH, and affects its sustainable use [10]. Incineration of waste plastics can generate electricity and heat [11], however, toxic compounds such as NO_2, SO_2 and dioxins are produced. Secondary recycling refers to the mechanical processing of waste plastics into products different from the original raw material. Compared with landfilling and incineration, secondary recycling is conducive to the management and resource utilization of waste plastics [12]. Nonetheless, current technologies of secondary recycling mainly convert waste plastics into raw polymeric materials of lower quality by shredding and grinding. For this reason, secondary recycling is called "downcycling", and the secondary plastic produced will still ultimately end up in landfill or incineration [13]. Overall, the current treatments of waste plastic are unsustainable, thus calling for more circular technologies.

In recent years, catalytic upcycling of waste plastics has emerged as a way to produce fuels or valuable chemicals, and also reduce environmental pollution [14]. A Web of Science search with 'upcycling' and 'plastic' as keywords shows that research on plastic upcycling increased exponentially from 2014 to 2023 (Fig. 2). The three main methods of catalytic upcycling are photocatalysis, electrocatalysis and thermocatalysis (Fig. 1). Thermocatalysis is done by pyrolysis, gasification, and hydrothermal treatments, which are conducted under high temperature and pressure to break chemical bonds and produce higher-value products such as fuels, e.g. H_2 and CH_4, and chemicals such as ethylene and

* Corresponding author.
E-mail address: wangchuanyi@sust.edu.cn (C. Wang).

terephthalic acid [15,16]. However, the use of expensive catalysts and large energy inputs in the process of thermocatalysis are considered as major obstacles to economic and environmental operation, especially in the context of reducing the utilization of fossil fuels. Besides the intensive energy demand, thermocatalysis has also the disadvantage of generating many by-products. Compared with thermocatalysis, photocatalysis and electrocatalysis appear to be more sustainable as these methods can be carried out under environmental conditions, employing sunlight or electricity produced from renewable sources [17,18]. Moreover, photocatalysis and electrocatalysis can activate and split chemical bonds more precisely, thus preserving other polymeric functional groups, and therefore, improving product selectivity [19,20]. Given this, Xie's group reviewed advanced plastic processing techniques, which are conducted under violent or mild conditions, including pyrolysis, hydropyrolysis, solvolysis, photocatalysis, electrocatalysis, and biocatalysis [6]. Zhao and co-workers summarized the investigation progress and critical design principles of photo-/electro-catalyst for the efficient conversion of plastics waste by breaking the chemical bonds selectively [21]. Combined processes, which are also driven by renewable energy such as photoelectrochemical (PEC) and solar thermal electrochemical process (STEP), have been studied in the catalytic field for decades as powerful tools [22–25], while few of reported reviews focus on PEC and STEP processes of plastics upcycling. Therefore, these processes, which appear promising for plastic upcycling, should be summarized in detail. In addition, the strategies of various raw plastic pretreatment are also significantly important, which are the prerequisite step of plastics conversion.

Herein, we review pretreatment methods for plastics upcycling, and the state-of-the-art plastic upcycling strategies by photocatalysis, electrocatalysis, photoelectrochemical catalysis and solar thermal electrochemical process. These methods allow to convert plastics such as polyethylene terephthalate [26,27], polyethylene [28], poly(lactic acid) [29], polyurethane [26] and polypropylene [28] into fuels and high-value chemicals. In addition, the catalytic mechanisms and conditions for various plastics upcycling are discussed and summarized. Finally, we propose a short conclusion, challenges and future perspectives on more feasible strategies for the plastics upcycling. We hope that this review enables a profound understanding of the concept and conversion mechanism in plastic disposal and provides some reference value for the design of subsequent catalytic materials.

2. Plastic pretreatment

Plastics are polymers and thus commonly present the characteristics of insolubility and chemical inertness, which hinder the interaction between the catalysts and plastics, further limiting the catalytic activity in photo-/electrocatalytic processes [30,31]. Therefore, before plastics upcycling, the pretreatment processes of plastics are essential. Plastics waste can be divided into four main types, including polyolefins, polyesters, polyurethanes and polyamides, which are linked by C—C, C—O, N—C—O and C—N, respectively.

Polyethylene (PE) is typical polyolefin plastic, and the main treatment methods for PE waste are based on physical methods and hydrolysis. Physical methods, such as cutting and ball milling, increase the specific surface area of plastics and thus favor the contact of plastics and catalysts. Physical pretreatment methods for PE plastics are simple to

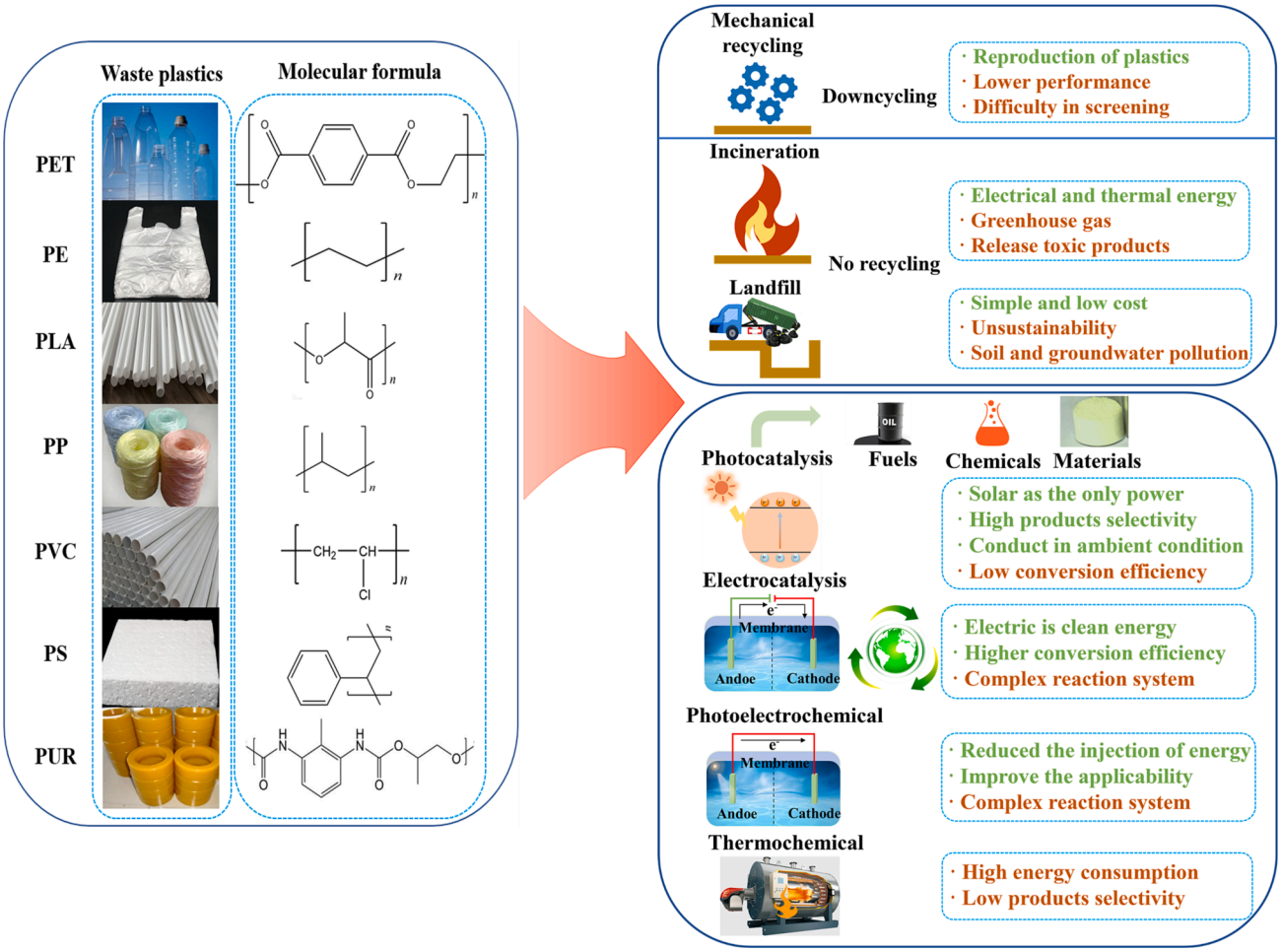

Fig. 1. Strategies to dispose waste plastics.

implement, exhibit high processing efficiency, and minimal environmental impact, but they still face the challenge of plastics' insolubility and chemical inertness. The insolubility in water and chemical inertness of PE results from the high dissociation energy of the C—C bond (~372 KJ/mol). Therefore, the conversion of PE pretreated by physical methods should use the photocatalysts with high oxidation potential, e.g., ZnO, Nb_2O_5, and $BiVO_4$. Given this, Xie and co-workers mixed pulverized commercial single-use bags or food wrap films with Nb_2O_5 for promoting the conversion of real-world plastics into CH_3COOH [28]. Besides, the main chemical methods for PE depolymerization involve elevated levels of acids and bases. For instance, Qiu's group reported that C—C bond of PE can be selectively broken to generate a range of carboxylic acids at 180 °C, owing to the strong oxidizing property of HNO_3. Afterwards, the generated acetic acid was oxidized selectively by photogenerated holes to produce methane [32].

Polyethylene terephthalate (PET) and polyurethane (PUR) are linked by C—O and N—C—O bonds, respectively. Depolymerization of these polymers are achieved by nucleophilic attack of the carbonyl to generate monomers. Reisner reported PET can be broken at ester bonds and converted into terephthalate (TPA) and ethylene glycol (EG) monomers in alkaline solution [26,29,33]. Terephthalate can then be directly recycled as an industrial raw material. Ethylene glycol can also be converted into formate and glycolic acid through photocatalytic and photoelectrochemical conversion. Besides, PUR is mainly hydrolyzed to 2,6-diaminotoluene and propylene glycol, whereas the propylene glycol components are converted into formate and pyruvate by photocatalysis. 6-Nylon, a polyamide linked by C—N bonds, can be depolymerized using ionic liquids to give monomeric lactam at 300 °C with a high yield [34].

In conclusion, pretreatment of plastics is crucial in the process of plastics upcycling. However, most methods involve the depolymerization of plastics in strong alkali, strong acid conditions or organic solvents, which will greatly increase the cost and may cause additional environmental issue. Therefore, conversion of plastics by biological methods is attracting more attention owing to their eco-friendly capacity based on the decomposition ability of proteases. For instance, using a modified PET protease, 94.9 % TPA was recycled with a purity of 97 % at 50 °C [35]. Accordingly, depolymerization reactions for polymers by biological methods with high conversion efficiency and selectivity to corresponding monomer products, presenting enormous potential for converting plastics waste to value-added molecules. Afterwards, the conversion of various plastics through photocatalysis, electrocatalysis, photoelectrochemical catalysis and solar thermal electrochemical process will be discussed in the following sections.

3. Photocatalysis

Heterogeneous photocatalytic systems consist basically of three steps: first, the semiconductor material is photoexcited yielding electrons and holes, which then migrate to the surface of the photocatalyst, thus allowing redox reactions to occur [13,36]. There are two main types of photocatalytic conversion of plastics: photodegradation and photocatalytic upcycling.

The ultimate products of plastic photodegradation are CO_2 and H_2O [9,37,38]. Nonetheless, in a typical photocatalytic upcycling process of plastics waste, which are selectively converted into value-added chemicals, meanwhile, H_2O is usually reduced into H_2 by the photoelectrons generated in photocatalysts [32,39]. Therefore, compared with photodegradation, photocatalytic upcycling of waste plastics both alleviates plastic pollution, and has huge economic benefits. For example, research in plastic upcycling has allowed to produce fuels, e.g. H_2, chemicals [40], e.g. formic acid, acetic acid, ethylene, and ethane, along other materials [41,42] such as functionalized plastics by photocatalytic. Table 1 presents reaction conditions for photocatalytic conversion of polyethylene terephthalate, polyethylene, polylactic acid, polypropylene, polyvinyl chloride, polyethylene glycol, polyurethane and polyacrylamide into H_2, a clean fuel, along with a valuable oxidation product.

3.1. *Photoreforming to produce hydrogen*

Photocatalytic water splitting to produce molecular hydrogen (H_2), has been explored for half a century [49,50]. Hydrogen is viewed as an ideal fuel because the only product of H_2 combustion is water, with few pollution [51–53]. The required potential energy for the production of H_2 by plastic photoreforming is nearly energy neutral and much lower than that for photocatalytic water splitting (1.6 eV) [54,55]. This is due to the lower potential needed for plastic oxidation in contrast to H_2O oxidation into O_2 [56,57]. Therefore, plastics can be regarded as sacrificial agents that are preferentially oxidized in the process of photocatalytic water splitting, thus reducing the integral potential needed for H_2 production [58,59].

In 1981, an early study by Kawai and Sakata has employed a platinized TiO_2 photocatalyst to reform PVC into H_2 at ambient conditions [46]. Although the catalyst activity was low for H_2 generation, this study provided inspiration for subsequent studies. Reisner et al. emphasized that photoreforming requires four components: a photocatalyst, a substrate, sunlight and water [26,29]. In 2018, they have used CdS/CdO_x quantum dots for photoreforming waste plastics to produce H_2 under visible light irradiation. Various plastics were tested, such as PET, PLA,

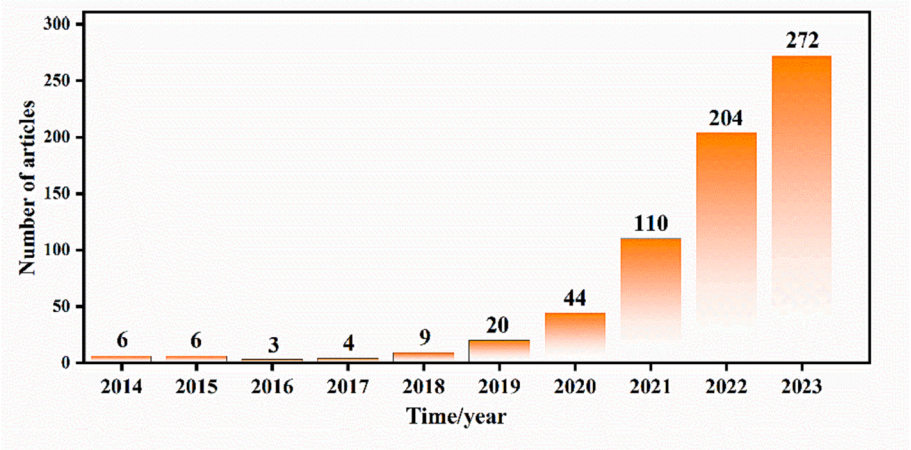

Fig. 2. Number of publications related to plastic upcycling, from a search in the Web of Science using the keywords 'upcycling' and 'plastic' from 2014 to 2023 on December 1, 2023.

Table 1
Conversion of plastics into fuels and chemicals.

Plastics	Catalyst	Solvent	Reduction product	Activity/ μmol $g^{-1}h^{-1}$	Oxidation product	Activity/ μmol $g^{-1}h^{-1}$	Ref.
Pre [a]-PET[b]	CdS/CdO_x	10 M NaOH	H_2	3.42×10^3	formate	–	[26]
PET	$Co\text{-}Ga_2O_3$	Deionized water	H_2	0.384×10^3	CO	100.6	[43]
Pre-PET	$CN_x\|Ni_2P$	1 M KOH	H_2	25.7	formate	–	[29]
Pre-PET	Ag_2O/Fe-MOF [c]	Deionized water	H_2	1.9×10^3	–	–	[44]
Pre-PET	MXene/ $Zn_xCd_{1-x}S$ [d]	10 M NaOH	H_2	14.17×10^3	formate	–	[45]
Pre-PET	MoS_2/CdS	10 M KOH	H_2	3.90×10^3	formate	5.96×10^3	[32]
PE [e]	$Co\text{-}Ga_2O_3$	Deionized water	H_2	0.647×10^3	CO	158.3	[43]
Pre-PE	Ag_2O/Fe-MOF	Deionized water	H_2	1.7×10^3	–	–	[44]
Pre-PE	Pt/TiO_2	5 M NaOH	H_2	31	–	–	[46]
Pre-PE	MoS_2/CdS	6 wt% HNO_3	H_2	1.13×10^3	CH_4	113.2	[32]
PE	Nb_2O_5	Deionized water	CH_3COOH	0.79×10^3	CO_2	–	[28]
Pre-PE	P25|Pt	6 wt% HNO_3	H_2	66	C_2H_6	0.26	[47]
PE	VPOM/CNNS [f]	CH_3CN	–	–	HCOOH	24.66	[48]
Pre-PLA [g]	CdS/CdO_x	10 M NaOH	H_2	64.3×10^3	pyruvate	–	[26]
Pre-PLA	$CN_x\|Ni_2P$	1 M KOH	H_2	55.7	CO_3^{-2}	–	[29]
Pre-PLA	MoS_2/CdS	10 M KOH	H_2	6.68×10^3	formate	5.37×10^3	[32]
PP [h]	$Co\text{-}Ga_2O_3$	Deionized water	H_2	64	CO	147.2	[43]
PP	Nb_2O_5	Deionized water	CH_3COOH	0.68×10^3	CO_2	–	[28]
PP	VPOM/CNNS	CH_3CN	–	–	HCOOH	26.68	[48]
Pre-PVC [i]	Pt/TiO_2	5 M NaOH	H_2	15	–	–	[46]
PVC	Nb_2O_5	Deionized water	CH_3COOH	0.66×10^3	CO_2	–	[28]
PVC	VPOM/CNNS	CH_3CN	–	–	HCOOH	29.85	[48]
PEG [j]	Ag_2O/Fe-MOF	Deionized water	H_2	2.48×10^3	HCOOH	–	[39]
PEG	VPOM/CNNS	CH_3CN	–	–	HCOOH	208.65	[48]
Pre-PUR [k]	CdS/CdO_x	10 M NaOH	H_2	0.85×10^3	formate	–	[26]
PAM [l]	VPOM/CNNS	H_2O	–	–	HCOOH	156.57	[48]

[a] Pre: Pretreated.
[b] PET: polyethylene terephthalate.
[c] MOF: metal–organic-framework.
[d] M represents transition metal, X represents C/N element.
[e] PE: polyethylene.
[f] VPOM: $H_5PMo_{10}V_2O_{40}$; CNNS: g-C_3N_4 nanosheets.
[g] PLA: polylactic acid.
[h] PP: polypropylene.
[i] PVC: polyvinyl chloride.
[j] PEG: polyethylene glycol.
[k] PUR: polyurethane.
[l] PAM: polyacrylamide.

PUR, PE and PVC. PLA, PET and PUR exhibited high activities with H_2 generation of 64.3, 3.42 and 0.85 mmol $g_{Cds}^{-1}h^{-1}$ in 10 M aq. NaOH, respectively. In addition, the monomers formed by alkaline hydrolysis of plastics were oxidized into high-value chemicals such as pyruvate, formate, ethanol, acetate and lactate. In the experiment of a real-world PET water bottle, the activity towards H_2 generation was 4.13 mmol $g_{Cds}^{-1}h^{-1}$ with a rate of conversion of 5.15 % and an external quantum yield of 2.17 % in 6 days. In this work, none of the polymers gave a conversion rate higher than 40 %, but this represented a proof-of-concept system to recycle waste plastics.

Because of the toxicity of Cd^{II} ions, the same research group designed a $CN_x|Ni_2P$ co-catalyst [29], made with cyanamide-functionalized carbon nitride (CN_x) and nickel phosphide (Ni_2P) for the photoreforming of plastics (Fig. 3a). Scanning electron microscopy (SEM) and transmission electron microscopy (TEM) analyses showed Ni_2P nanoparticles with a diameter of 9.4 ± 0.6 nm distributed across the CN_x surface (Fig. 3b). This allowed higher electron-hole separation due to a shift of electron density from CN_x to Ni_2P in $CN_x|Ni_2P$. Therefore, $CN_x|Ni_2P$ showed high photoreforming efficiency. For example, H_2 evolution varied from 82.5 ± 7.3 and 178 ± 12 μmol g_{sub}^{-1}, after 50 h of photoreforming of PET and PLA, respectively (Fig. 3c). Here, H_2 was derived from water molecules rather than from plastics as evidenced by the isotope labeling. The ^1H NMR spectra proved ethylene glycol (EG) and lactate were hydrolysates of PET and PLA, which were mainly converted into formate and CO_3^{2-}, respectively. (Fig. 3d-f). Moreover, the practical efficacy was evaluated through long-term photoreforming of polyester microfibers, a PET bottle, and oil-contaminated PET. SEM showed developed cracks and pits on the microfibers. After 5 days of illumination, H_2 production was 104, 22, and 11.4 μmol g_{sub}^{-1} for polyester microfibers, PET bottles, and oil-contaminated PET, respectively. For future large-scale applications, they upscaled the photoreforming device from 2 to 120 mL. When the conditions were optimized, the biggest setup exhibited a H_2 production of 0.53 μmol cm^{-2}, which was higher than that for the smallest setup (0.26 ± 0.03 μmol cm^{-2}). That is to say, a 15 m^2 reactor would be enough to power a smartphone.

To stimulate the maximum activity of the photocatalyst and prevent clumping, Reisner's group designed a photocatalyst panel [60], which could attach the $CN_x|Ni_2P$ power to frosted glass (Fig. 3g). The yield of H_2 was positively correlated with the amount of catalyst at low load, and the yield tended to be flat at high load (Fig. 3h). Interestingly, the photocatalytic panel showed higher H_2 production activity when light irradiated from the back side, which is explained by an inner filter effect promoted by the solution in case of the front side irradiation [60]. Finally, the photocatalytic panel along with $CN_x|Ni_2P$ could convert high concentrations of PET-colored solutions in the flow photoreforming system (Fig. 3i). This work overcomes the use of toxic materials, and analyzes the photoreforming process of PET and PLA, systematically. Moreover, the development of photocatalytic panel made photoreforming of plastic coloring solution possible, laying a foundation for the practical application of subsequent plastic upcycling.

Recently, metal organic frameworks (MOF) have been widely explored in photocatalysis, because of their large surface area and excellent light absorption properties [61]. However, the low charge separation efficiency limits the application of MOF materials. For this reason, Zhang et al. constructed a Ag_2O/Fe-MOF heterojunction to enhance the separation efficiency during photocatalytic conversion of

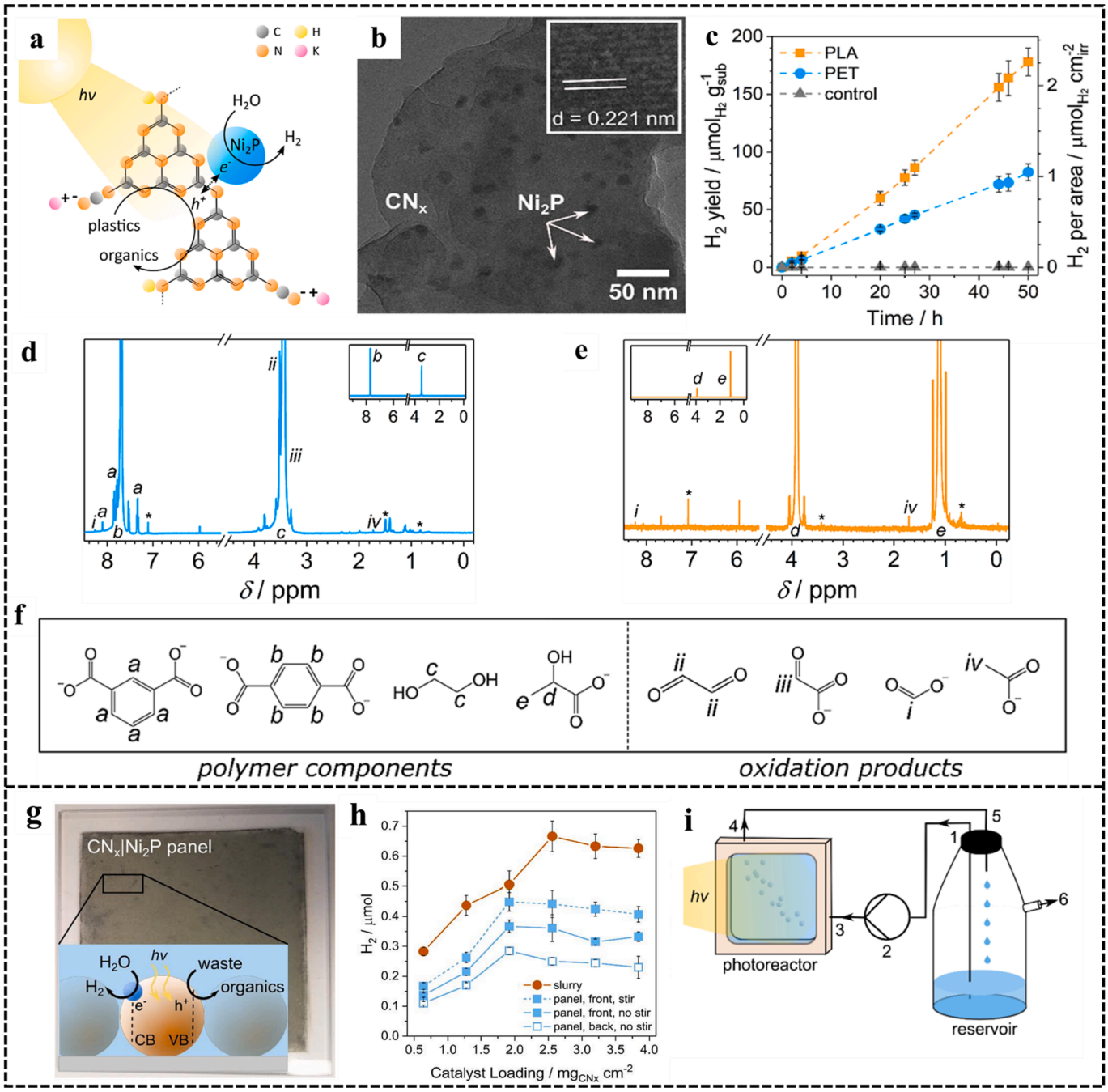

Fig. 3. (a) Photoreforming plastic and (b)TEM image of the $CN_x|Ni_2P$ (2 wt%). (c) The stability experiment of photoreforming PET and PLA in 1 M KOH under simulated sunlight. ^{1}H NMR spectra of photoreforming PET (d) and (e) PLA. (f) Chemical structures and peak assignments. Reproduced with permission [29]. Copyright 2019, American Chemical Society. (g) Photoreforming upscaled panel for 25 cm^{-2} loading with $CN_x|Ni_2P$. (h) The H_2 activity in different catalyst loading. (i) Schematic diagram of expanded photoreforming device in the flow phase. Reproduced with permission [60]. Copyright 2020, John Wiley and Sons.

microplastics (PEG, PET, PE) into valuable chemicals and H_2 (Fig. 4a and b) [44]. The H_2 production of pure Ag_2O, Fe-MOF, Ag_2O/Fe-MOF, Ag_2O@Fe-MOF (physical mixed) and Ag_2O-Fe-MOF was evaluated by the photocatalytic conversion of PEG and Ag_2O/Fe-MOF (0.2 wt%) presented the highest H_2 production of 6.2 mmol g^{-1}, and 27.5 mg of PEG microplastics were converted in 3 h (Fig. 4c and 4d). Mechanistic investigation showed that when Ag_2O and Fe-MOF were in close contact, the Fermi level of Ag_2O increased and the Fermi level of Fe-MOF decreased until the Fermi levels of Ag_2O and Fe-MOF converge. This led to the overall shift of Ag_2O energy band and the formation of p-n junction along with an internal electric field. Under irradiation, the electrons of Ag_2O and Fe-MOF were excited to their respective conduction bands, and the electrons of the Ag_2O conduction band migrated to the conduction band of Fe-MOF. At the same time, the holes of Fe-MOF were transferred to the valence band of Ag_2O in the action of the internal electric field. Finally, electrons accumulated in the conduction band of Fe-MOF to reduce water into H_2, and holes accumulated in the valence band of Ag_2O to oxidize water to •OH radicals and further oxidize microplastics to short-chain organic molecules (Fig. 4e). This work constructs a Ag_2O/Fe-MOF heterojunction through a novel in-situ synthesis method, enables Ag_2O nanometer-sized particles were confined into the framework of MOFs with uniform size ~ 6 nm, provides more active sites for photoreforming of plastics.

Syngas is made of CO and H_2, which are important industrial

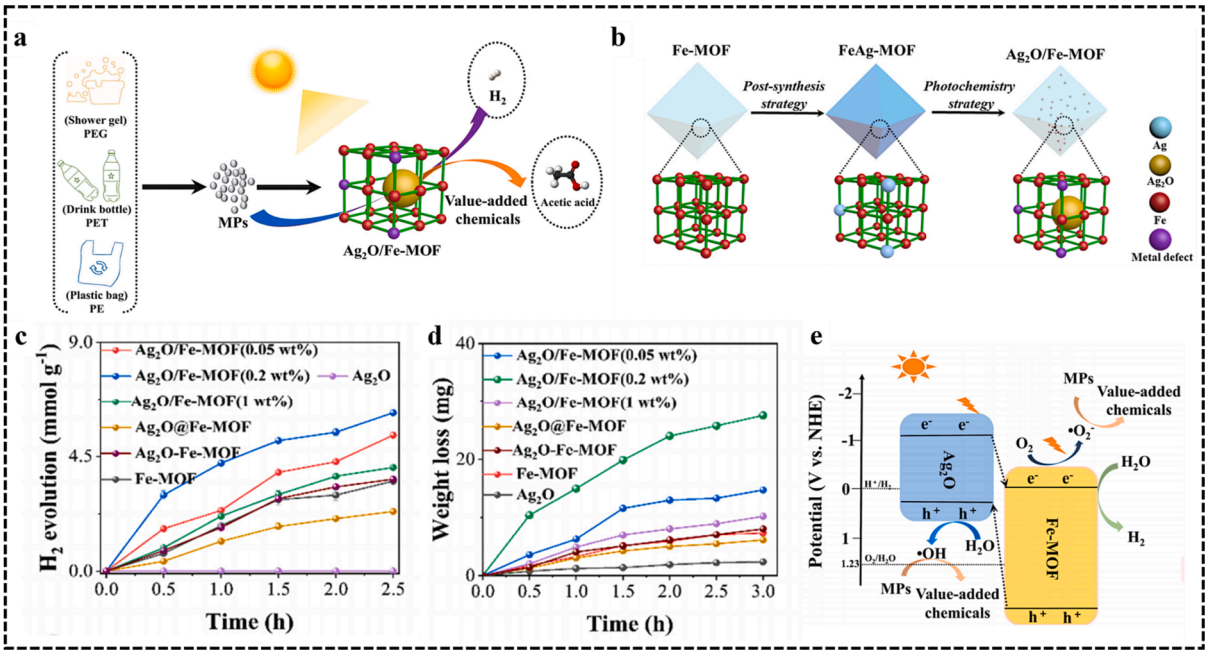

Fig. 4. (a) Ag_2O/Fe-MOF photoreforming of various plastics and (b) in situ synthesis processes of Ag_2O/Fe-MOF. (c) The H_2 production and (d) weight loss in the process of photoreforming polyethylene glycol (PEG) under simulated sunlight with different catalysts. (e) The reaction mechanism of Ag_2O/Fe-MOF photoreforming microplastics [44]. Copyright 2022, Elsevier.

chemicals since they could act as feedstocks for synthesizing hydrocarbon fuels [62,63]. Xie et al. put forward utilizing Co-Ga_2O_3 nanosheet photocatalysis to convert waste plastics (PE, PP and PVC) into H_2 and CO under ambient conditions (Fig. 5a). The electrons and holes of Ga_2O_3 have strong redox performance, due to its negative conduction (−1.62 V vs. NHE) and positive valence band potential (+3.16 V vs. NHE), so that the photogenerated carriers of Ga_2O_3 could satisfy the thermodynamic demand for promoting most of the redox reactions of interest [43,64]. Compared with pure Ga_2O_3, Co-Ga_2O_3 had more efficient photocarrier separation efficiency (Fig. 5b), stronger light absorption (Fig. 5c) and stronger adsorption performance for CO_2, which were conducive to the reduction process of carbon dioxide. Thus, Co-Ga_2O_3 nanosheets showed higher photoconversion activity of PE, PP and PVC. For example, the activities of Co-Ga_2O_3 converted PE plastic bags into H_2, CO and CO_2

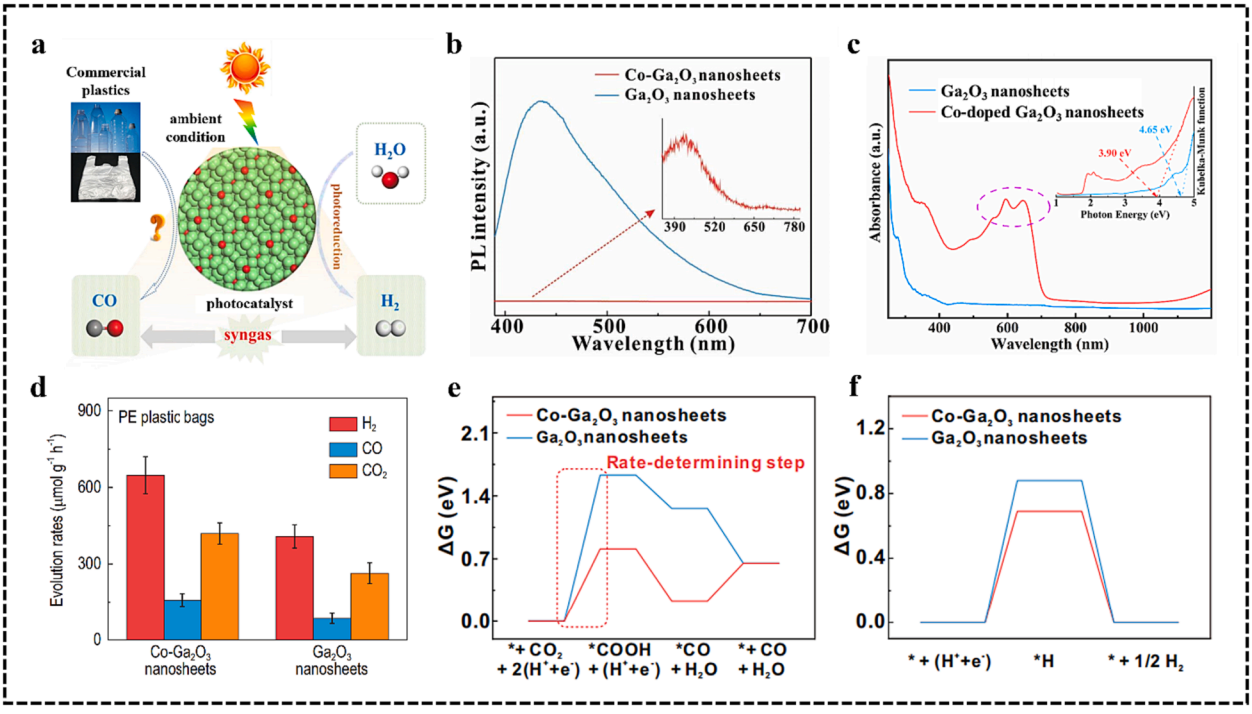

Fig. 5. (a) Photoconversion of various plastics into syngas. (b) PL spectra and (c) UV–vis diffuse reflectance spectra for the Ga_2O_3 nanosheets and the Co-Ga_2O_3 nanosheets. (d) The activity of H_2, CO, CO_2 in photoreforming commercial PE plastic bags in 100 mL deionized water. The Gibbs free energies (ΔG) of Co-Ga_2O_3 and the Ga_2O_3 nanosheets (e) photocatalytic CO_2 to CO and (f) H_2O to H_2 [43]. Copyright 2022, Oxford University Press.

were 647.8, 158.3 and 419.3 μmol $g^{-1}h^{-1}$ (Fig. 5d), individually. Meanwhile, the activities of pure Ga_2O_3 were 404.9, 83.3 and 262.1 μmol $g^{-1}h^{-1}$. Moreover, the total reaction could be divided into three steps:

- Step 1: H_2O was split into H_2 and O_2 by part of the photogenerated charge carriers.
- Step 2: The plastic was degraded into CO_2, while O_2 was gradually reduced into $O_2^{\bullet-}$, H_2O_2 and H_2O.
- Step 3: CO_2 was reduced to •COOH intermediates and further to CO, while H_2O was oxidized to O_2.

Among these three steps, the formation of •COOH and H* intermediates are the rate-limiting steps and both of the energy barriers of Co-Ga_2O_3 to form •COOH intermediates and H* were lower than that for pristine Ga_2O_3 by calculating the Gibbs free energy of the reaction (Fig. 5e and 5f). Therefore, Co-Ga_2O_3 exhibited higher activity than Ga_2O_3 during the photocatalytic conversion of PE. Although the conversion efficiency of PE in this work is still far from practical application, the photoreforming of plastics to produce syngas in water solution under environmental conditions is successfully proven. Moreover, the rate limiting step of the process is obtained through a mechanism exploration, which provides reference and guidance for the design of high-efficient catalysts in the future.

3.2. Photocatalytic conversion of plastics into carbon-containing chemicals

Most plastics are derived from petroleum-based hydrocarbons [65,66].Therefore high-value chemicals can be easily produced by cracking waste plastic [67]. Photocatalytic conversion of waste plastics into chemical monomers not only reduces environmental pollution but also can alleviate the demand for fossil fuels [68]. Compared to photoreforming of waste plastics for H_2 production, photocatalytic conversion of waste plastics to high-value chemicals mainly depends on the oxidation processes of substrates [69]. The main barrier is the high stability of the C—C bonds in the polymer, which typically leads to slow kinetics and the low selectivity of the target product [70]. These problems can be overcome by selecting the appropriate band structure of the photocatalyst or adjusting the band position to obtain suitable redox potentials [71].

Formic acid is a common chemical, utilized as a disinfectant and preservative, as well as in fuel cells [72,73]. Li and co-workers reported a VPOM/CNNS Z-scheme, which was consisted of $H_5PMo_{10}V_2O_{40}$ (VPOM) and ultrathin g-C_3N_4 nanosheets (CNNS) through electrostatic interaction for photocatalytic conversion of plastics (PE, PP, PVC) into formic acid (HCOOH) under visible light conditions [48]. The morphology of VPOM/CNNS was still a curved sheet-like structure, after the introduction of VPOM, and it could be observed by aberration-corrected high-angle annular dark field TEM (AC-HAADF-STEM). VPOM nanoparticles were evenly distributed on the surface of CNNS to form a 0D/2D structure (Fig. 6a). In situ electron spin resonance (ESR) measurements confirmed that under the action of the internal electric field of VOPM/NNS, photogenerated electrons and holes were accumulated in the conduction band of CNNS and the valence band of VPOM, further reacted with O_2 and H_2O to produce $O_2^{\bullet-}$ and •OH, respectively (Fig. 6b and 6c). The valence band (E_{VB}) and conduction band (E_{CB}) potentials of CNNS and VPOM were 1.92, −1.04 V and 3.04, 0.85 V, respectively. Therefore, electrons could be transferred spontaneously between the interface of CNNS and VPOM to form the internal electric field of CNNS pointing towards VPOM (Fig. 6d and 6e). Consequently, VPOM/CNNS exhibited higher electron-hole separation efficiency and higher photocatalytic activity and the optimal VPOM/CNNS-15 sample showed the activity for HCOOH production was 24.66 μmol h^{-1} g^{-1} towards PE conversion. Moreover, the reaction mechanism was proposed, the C—C bond of PE was oxidized cleavage to form formaldehyde and alkyl radical. The alkyl radical was further oxidized into alkyl peroxide groups, long-chain alcohol and then participated in the next reaction of C—C bond cleavage. On the other hand, the aldehyde was oxidized into formic acid by $O_2^{\bullet-}$ (Fig. 6f). Briefly, this work realizes the high-efficient photocatalytic upcycling of plastic through constructing Z-scheme which exhibits efficient spatial separation and strong redox ability of photoexcited charge carriers, and expands the roads of Z-

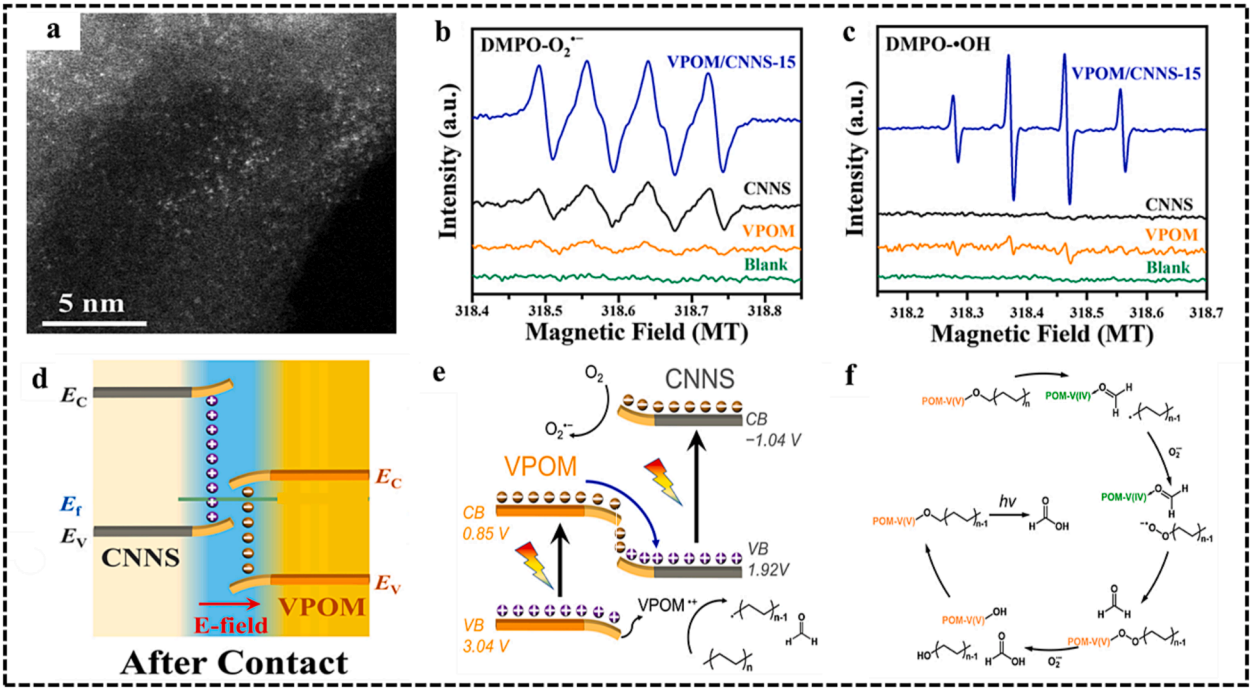

Fig. 6. (a) Aberration-corrected high-angle annular dark field TEM image of VPOM/CNNS-15 material. In situ ESR signal of (b) $O_2^{\bullet-}$ and (c) •OH of materials after 5 min of light. (d) VPOM/CNNS Z-scheme heterojunction after contact. (e) Diagram of photocatalytic upcycling waste plastic and (f) the reaction mechanism schematic of photocatalytic oxidative upcycle PE to formic over VPOM/CNNS Z-scheme heterojunction [48]. Copyright 2022, Elsevier.

scheme heterojunction in upcycling of plastic wastes.

Morphology is an important characteristic of photocatalysts because an appropriated morphology is beneficial to improve the separation efficiency of photogeneration carriers [74–76]. Qiu's group [32] realized the high-efficiency conversion of PET, PLA and PE to chemicals by MoS_2/CdS composite catalyst. MoS_2 covered one end of CdS nanorods to form an electron accumulation area and the other end formed a hole accumulation area (Fig. 7a). So that the electron-hole separation efficiency of MoS_2/CdS was improved. The anisotropic morphology of MoS_2/CdS was observed by SEM, while Pt nanoparticles and MnO_x nanosheets were selectively deposited on the end of CdS, which was covered by MoS_2, and the other end (Fig. 7c and 7d). The H_2 activity was 6.68 ± 0.10 mmol $g^{-1}h^{-1}$ and 3.90 ± 0.07 mmol $g^{-1}h^{-1}$ in the PLA and PET hydrolysate (10 M KOH) with the optimal load capacity of 21.8 wt %.

On the other hand, the oxidation half-reactions over MoS_2/CdS of PLA and PET were the conversion of the hydrolyzed monomers into formate and exhibited 5.37 ± 0.67 mmol/L and 5.96 ± 0.02 mmol/L in 5 h of photoreforming, respectively. Different from PLA and PET, PE was hydrolyzed to succinic acid and glutaric acid, in 6 wt% HNO_3 solution at 180 ℃ for 5 h (Fig. 7d). Moreover, CH_4 was generated by photo-oxidation decarboxylation of CH_3COOH achieved 196.2 μmol $g^{-1}h^{-1}$, meanwhile, ethane, propane and n-pentane were also produced due to the generation of carbon-centered radical species in the process of photoreforming PE. In this paper, composite photocatalysts are covered for the first time from the perspective of charge separation behavior for the upcycling of plastics, further paving the way for further study on plastic upcycling.

Reisner et al. also converted PE hydrolysate into alkane chemicals through photocatalysis [47]. The whole reaction could be divided into two steps. The first step was the hydrolysis of PE to produce 44 % succinic acid, 22 % glutaric acid, 22 % acetic acid, 9 % lipid and 4 % propionic acid in 6 % HNO_3 aqueous solution at 180 ℃ for 4 h. The second step was photocatalytic decarboxylation of succinic acid by hole to form propanoic acid intermediates which further react with H_{ads}/H_2 to produce ethane and CO_2. Similarly, glutaric acid was converted to propane. When pure succinic acid as substrate, P25|Pt and $^{NCN}CN_x$|Pt on the activity of ethane were 56.3 and 7.2 μmol $g_{cat}^{-1}h^{-1}$ (Fig. 7e), respectively. Besides, the PE hydrolysate solution was also tested with a P25|Pt catalyst and the products were ethane (0.25), ethylene (0.02), propane (0.14) and propylene (0.007 mmol g_{cat}^{-1}). Moreover, they investigated the activity of a photocatalyst in a flow phase using a photocatalyst panel, which was fixed to a ground glass surface and irradiated on the back of the photocatalyst panel to reduce the absorption of light by the substrate solution. The $^{NCN}CN_x$|Pt exhibited higher activity for ethane (77.9 μmol m^{-2}), ethylene (69.2 μmol m^{-2}), propane (40.7 μmol m^{-2}) and propylene (19.1 μmol m^{-2}). This work provides a breakthrough to closed-loop recycling of plastic through the conversion of plastic into gaseous alkane, which can be separated from the reaction solution, readily.

CH_3COOH is also a commonly used chemical product [77–79]. Xie et al. transformed PE, PP and PVC into CH_3COOH by a two-step method involving photocatalytic C—C bond cleavage and photoinduced C—C coupling, under simulated natural environmental conditions (Fig. 8 a) [28]. Because of the high stability and suitable band position Nb_2O_5 was selected as a photocatalyst, with the valence band maximum and conduction band minimum at + 2.5 V and at − 0.9 V (vs. NHE, pH = 7), respectively [80,81]. That is meaning the redox ability of photogenerated carriers of Nb_2O_5 can meet the potential demand for the conversion of CO_2 to CH_3COOH and the generation of •OH in water (Fig. 8 b). Taking PE as an example to explore its reaction mechanism, $AgNO_3$ was added into the reaction systems, then only CO_2 could be detected. It could infer that the C—C bond was oxidized to form CO_2, meanwhile, CH_3COOH and CO stemmed from the photoreduction processes. Moreover, •OH and $O_2^{\bullet-}$ radicals exhibited strong electron spin resonance (ESR) signals (Fig. 8c and 8d). On the other hand, a characteristic peak of H_2O_2 at 436 nm was observed by UV–vis absorption spectrum, indicating that photogenerated electrons of Nb_2O_5 could gradually reduce O_2 into $O_2^{\bullet-}$, H_2O_2 and H_2O. Furthermore, in situ FTIR spectroscopy demonstrated C=O and COOH were formed by the reduction of CO_2. On the whole, photocatalytic converted PE into CH_3COOH could be divided into two Steps (Fig. 8e):

-Step 1: PE was converted into CO_2 by •OH oxidation to break the C—C bond; in the meantime, O_2 was reduced by photogenerated electrons to $O_2^{\bullet-}$, H_2O_2 intermediates, and finally H_2O was formed.

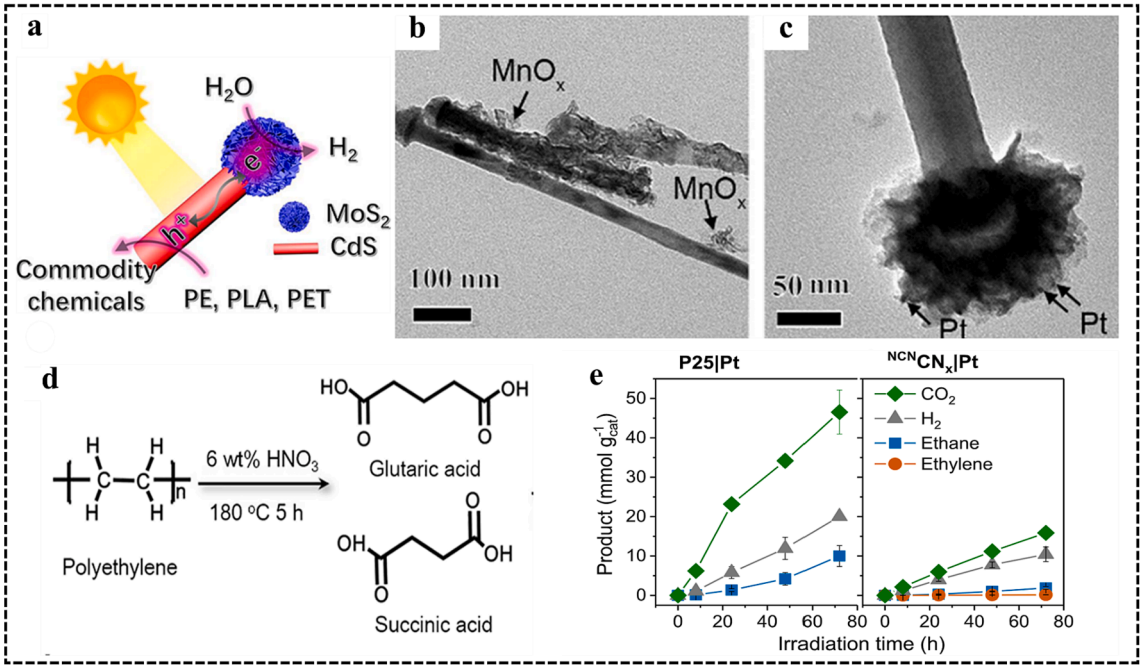

Fig. 7. (a) MoS_2/CdS photoreforming plastics. The investigation of the redox sites of MoS_2/CdS by selective light deposition of (b) MnO_x and (c) Pt. (d) Schematic diagram of PE hydrolysis process in HNO_3 solution [32]. Copyright 2022, American Chemical Society. The different products yield of (e) photocatalytic convert succinic acid and PE decomposition solution using a flow device over P25|Pt and $^{NCN}CN_x$|Pt [47]. Copyright 2021, American Chemical Society.

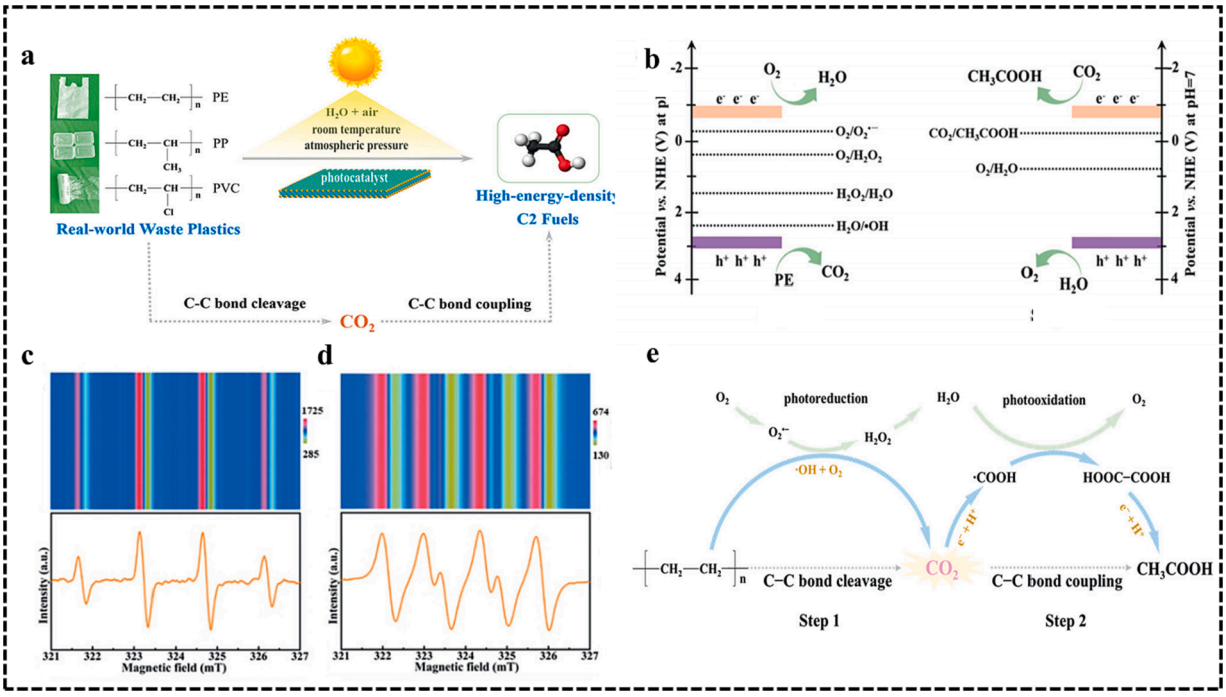

Fig. 8. (a) Photocatalytic conversion of plastics into C_2 chemicals by C—C bond cleavage and C—C coupling. (b) The band position of Nb_2O_5 and redox relative energy levels of CO_2, H_2O and O_2. ESR signal of (c) •OH and (d) $O_2^{\bullet-}$ during photoconversion PE process in pure water and methanol/water mixed solution. (e) The reaction mechanism of photoconversion PE process for C—C bond cleavage and coupling [28]. Copyright 2019, John Wiley and Sons.

-Step 2: Two •COOH intermediates reduced from CO_2 were photo-induced to form HOOC−COOH and were further reduced into CH_3COOH.

Pure PE, PP and PVC were treated in a simulated natural environment the total degradation within 40, 60, and 90 h, and the average activities of CH_3COOH in the degradation process were 47.4, 40.6, and 39.5 μg $g_{cat}^{-1}h^{-1}$, respectively. It should be noted that when CO_2 was passed directly into the solution as a substrate, the efficiency of photoconversion of PE, PP and PVC to CH_3COOH is similar to it, further implying that CH_3COOH was reduced from CO_2 by photocatalysis. Compared with other studies of plastics waste upcycling, this two-step method allows the coupling of oxidation and reduction to produce C_2 chemicals in water solution without further disposal of plastics and gives a new approach to upgrading and utilizing plastics.

Given unstable adsorption of the PE monomer, Xie and coworkers designed a photocatalyst exhibited charge-asymmetrical dual sites by doping Zr atom over $CoFe_2O_4$ [82]. The in situ FTIR spectra confirmed the formation of CH_3COOH was originated from the degradation of PE, directly. DFT calculations proved the charge-asymmetrical dual sites (Zr−Fe) were constructed by doping Zr atom which exhibited low-electro-negativity over $CoFe_2O_4$. As a result, the optimized showed the CH_3COOH evolution rate of 1.10 mmol $g^{-1}h^{-1}$ with the help of 3 % H_2O_2 which could promote the generation of •OH radicals. This work constructs charge-asymmetrical dual sites photocatalyst through doping different negativity atoms, realizes the conversion of PE into CH_3COOH with high formation rate and 100 % selectivity under normal temperature and pressure.

3.3. *Photocatalytic functionalization of plastics*

In addition to the depolymerization of plastics into small molecular monomers, the post-polymerization functionalization captured the researcher's attention [83–85]. The advantage of the functionalization of plastics is that the process does not require the breaking of the polymer backbone chain, and the installation of functional groups directly onto the polymer long chain molecules gives the polymer unique properties [86].

Polystyrene (PS) is difficult to dispose of, due to its strong chemical stability [88–90]. Leibfarth [87] reported a method for the C—H functionalization of PS by the use of their innate reactivity with electrophilic radical intermediates. The fluoroalkylation of PS could be divided into two steps in which, the first was the electronic reduction of $Ru(bpy)_3Cl_2$ trifluoroacetic anhydride into electrophilic trifluoroalkyl radicals, pyridine and CO_2. The second step, trifluoroalkyl radicals would be installed on the aromatic rings of PS by replacing H (Fig. 9a). In optimal, trifluoromethylation of PS reached 32 ± 2 $_{mol}$ %, and by changing the stoichiometric ratio of pyridine-N-oxide to trifluoroacetic anhydride (TFAA) the degree of trifluoromethylation of PS can be adjusted while the molecular weight distribution (MWD) of original PS was preserved (Fig. 9b). Besides, the contact angle between pure PS and water was 94° and the highest was 111° after fluoridation (Fig. 9c), indicating that fluoridation of PS increased its hydrophobicity, and fluoroalkylation could be applied to other aromatic-containing polymers like polyesters and polycarbonates.

However, the content of ruthenium (Ru) found in the crust is only one billionth of the total mass, therefore it is an extremely precious metal element. Therefore, the utilization of Ru-based catalysts is not economically viable [91,92]. Leibfarth and co-workers took advantage of organic photocatalysts namely phenoxazine, phenothiazine, and phenazine instead of $Ru(bpy)_3Cl_2$ to achieve the fluoroalkylation of aromatic-containing polymers under environmental conditions (Fig. 9d) [42]. Phenoxazines and phenothiazine showed a high proportion of fluoroalkylation (20 % and 19 %), but both of them accompanied by chain-coupling side reactions resulted in the MWD of the products was changed. Meanwhile, phenazine photocatalysts not only achieved 18 % fluoroalkylation but also did not affect the MWD of the product when the reactant concentration was 0.4 M and the catalyst load was 1 $_{mol}$ % (Fig. 9e and 9f). Moreover, by adjusting the stoichiometric ratio of pyridine N-oxide and TFAA, the functionalization of the polymer reached 33 $_{mol}$ %. C-H fluoroalkylation could also be achieved by organic photocatalysis of post-consumption and post-industrial PS waste, and this method could be used for the fluoroalkylation of

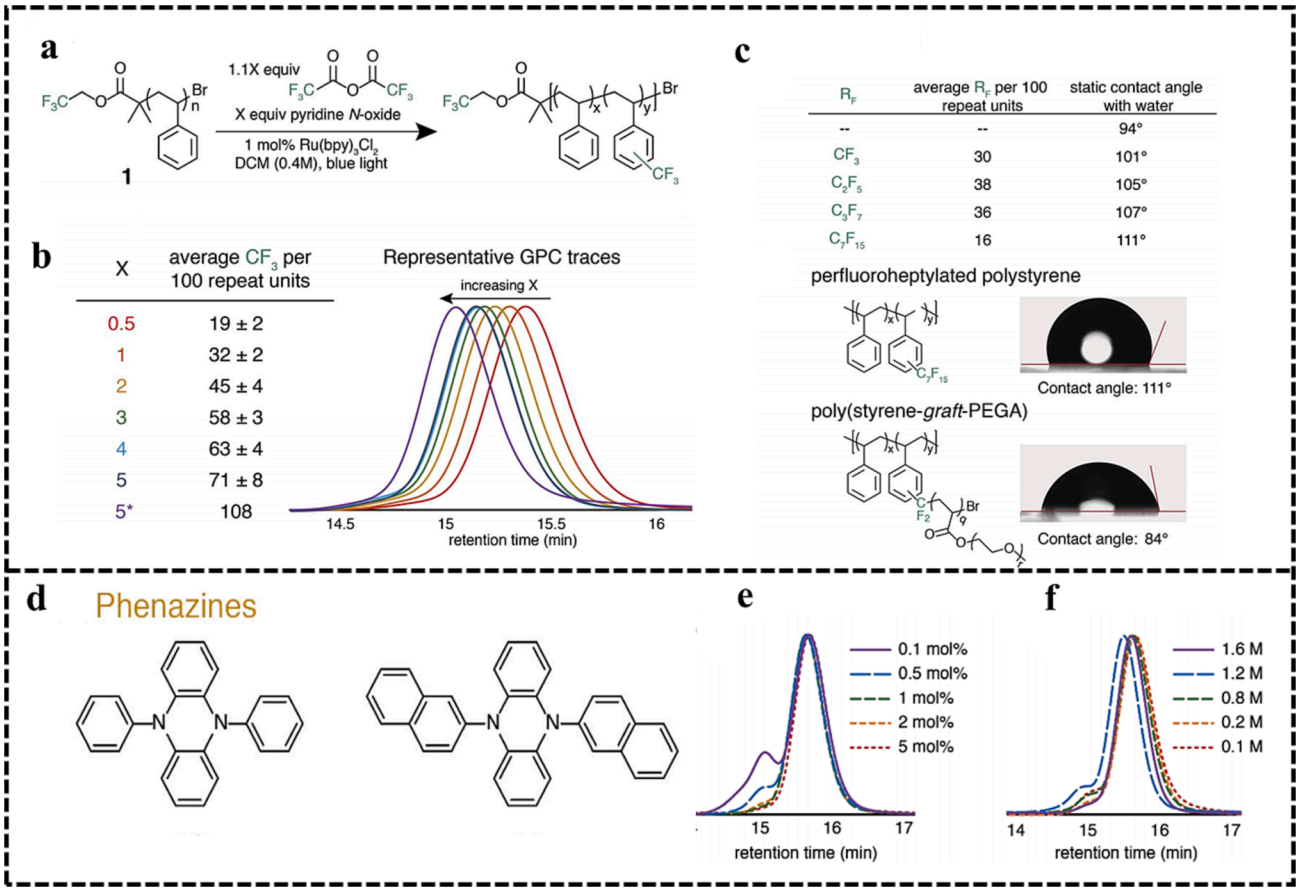

Fig. 9. (a) Schematic diagram of photocatalytic trifluoromethylation of PS over $Ru(bpy)_3Cl_2$. (b) The trifluoromethylation of PS in different proportions of pyridine N-oxide and trifluoroacetic anhydride. (c) Contact Angle between water and PS at different degrees of trifluoromethylation [87]. Copyright 2019, The Royal Society of Chemistry. (d) Phenazine catalysts were used in the study. GPC traces from the trifluoromethylation of different (e) catalyst loading and (f) concentrations of reactants [42]. Copyright 2020, The Royal Society of Chemistry.

polyester, proved the applicability of C–H in various plastics. This work demonstrates the value of the methods developed and the structure–reactivity relationships identified in facilitating the continued adoption of C-H functionalization methodologies that improve the properties of commercially available polymers.

4. Electrocatalytic

4.1. Electrocatalytic for plastics upcycling

Although electric energy is secondary energy, with the gradual maturity of clean energy generation technology, electric energy is also considered to be sustainable energy [93–96]. Thus, electrocatalysis technology has attracted extensive research [97,98], such as electrocatalytic water splitting and the reduction of CO_2 into CO, HCOOH, CH_3OH, etc [99,100]. Recently, more reports focus on electrocatalytic upcycling of plastics waste and exhibited great potential for the industrial application. In a typical electrocatalytic upcycling process of plastics waste, an external bias is applied to facilitate the redox reaction, allowing access to the reaction pathways. Generally, the oxidation of plastics waste and the reduction reaction of water occur at anode and cathode electrodes, which are connected by an external electric circuit and an electrolyte in-between. In view of this, electrocatalytic technology exhibits some obvious advantages for the conversion of plastic waste, including a controllable electrode potential operation process, recyclable supporting electrolytes to reduce overall chemical consumption. Therefore, the utilization of electrocatalytic technologies to upcycle the plastics waste is promising [101–104]. The products obtained by electrocatalysis can be divided into solid carbonaceous materials and value-added chemicals. In this part, we would focus on assessing the study about value-added chemicals, because in the formation of solid carbonaceous materials pyrolysis plays a major role, which is not in line with the concept of clean energy.

Table 2 shows some of the previous examples of the electrocatalytic upcycling of plastics. In general, the anode material is optimized first, because the upgrading and conversion of plastics are mainly oxidation reactions [110]. Therefore, Chen et al. constructed two-electrode electrolysis cell using a Ni foam (NF) catalyst modified by Pd as an anode, and NF as a cathode [107]. The PET bottle could be oxidized to carbonate and terephthalate at the anode, meanwhile, the water was reduced to H_2 at the cathode in 1 M KOH solution. The Pd/NF-10 showed network structure and exhibited better electro chemical performance because Pd/NF-10 exposed more catalytically active sites than others. The electro-reforming experiment was conducted in the optimum condition, all the PET was converted into terephthalate and carbonate after 20 h and the pathway of reaction was proposed for EG oxidation. The yield of terephthalate reached up to 99 % and the faradaic efficiency of carbonate reached 93 %. Moreover, the stability also was tested, and after 4 cycles it retained high selectivity and FE. Besides, the real-world PET bottle was also converted into terephthalate and carbonate with high selectivity and faradaic efficiency (FE). At the same time, H_2 was generated at the cathode with high FE reached 98 %. Although this work can achieve a complete conversion of PET, the added-value of carbonate, one of the products, is not enough.

Compared with carbonate, the added value of formic acid is higher due to it is one of the basic organic chemical raw materials widely used

Table 2
Examples of electrocatalytic upcycling of waste plastics.

Plastic type	Electrolyte	Applied potential	Anode/Cathode	Anode product	Faradaic efficiency	Cathode product	Faradaic efficiency	Ref.
[a]Pre-PET	0.1 M KOH	1.45 V	CuO/Pt	formate	88 %	H_2	–	[105]
Pre-PET	1 M NaOH/1 M $NaHCO_3$	1.9 V	$NiCo_2O_4/SnO_2$	formate	85 %	formate	70 %	[106]
Pre-PET	1 M KOH	0.7 V	Pd-NF/NF[a]	CO_3^{2-}	91 %	H_2	98 %	[107]
Pre-PET	2 M KOH	1.5 V	$CoNi_{0.25}P$/ $CoNi_{0.25}P$	formate	96.7 %	H_2	–	[108]
Pre-PET	1 M KOH	1.2 V	Pd NTs/LC-CoOOH	glycolic acid	81.17 %	NH_3	94.47	[109]
Pre-PE	NaOH pH = 10	5 V	Carbon Paper/Pt	C_2H_4	3.8 %	H_2	100 %	[47]
Pre-PE	2:1 Methanol pH = 10	5 V	Carbon Paper/Pt	C_2H_4	9.0 %	H_2	65.3 %	[47]

[a] Pre: Pretreated.

in pesticide, leather, dye, medicine and rubber industries [111–113]. Recently, Zhao and co-workers [105] reported CuO nanowires (NW) electrocatalysis conversion of PET hydrolysate into formate (Fig. 10a). TEM images demonstrated that CuO NW was synthesized by an in situ self-growth method (Fig. 10b), successfully. Electrochemical tests showed that CuO NWs-200 °C electrode exhibited the optimal electrochemical performance, which was manifested in lower onset oxidation potentials, Tafel slope, transfer resistance and higher double-layer capacitance compared with other electrodes. In a typical experiment, 1 M KOH with 0.1 M PET hydrolysate was electrolyzed, formic acid was generated on the anode CuO, and H_2 was generated on the cathode Pt. Moreover, because ethylene glycol (EG) was the main product of PET hydrolysate, 10 mM pure EG was electrolyzed in 0.1 M KOH solution. After 62C, the faradaic efficiency and yield of formate were 88 % and 86.5 %, respectively. Besides, the DFT calculation suggested a possible reaction pathway, first EG adsorbed on the surface of CuO through a bidentate configuration, then the two O-H bonds of EG were broken to form $*OCH_2CH_2O*$ intermediates, further formed *OCH − HCO*, and finally the C—C bond cleavage to generate formic acid (Fig. 10c and 10d). This work presents a novel way of electro-reforming PET waste through utilizing CuO NWs electrode to produce valued chemicals and H_2, and proposes the possible pathway of pretreated PET oxidation reaction.

Besides, Duan's group reported electrocatalytic upcycling of PET into potassium diformate (KDF) and terephthalic acid (TPA) [108]. PET was decomposed into PTA and EG in 1 M KOH solution, and then the EG was further oxidized into formate. The next step was the acidification of PET hydrolysate by adding formic acid to obtain the PTA and KDF. Ni_2P and CoP nanoparticles were interconnected with each other observed through HRTEM, indicating that heterojunctions were formed in the $CoNi_{0.25}P$ electrode [114,115]. Compared with other traditional electrodes (Pt/C, RuO_2 and Ni-Fe/NF), $CoNi_{0.25}P$/NF electrode had an excellent electrochemical performance in all aspects, and the comprehensive performance is optimal in EG oxidation and H_2 evolution. In a three-electrode system, with or without EG in the electrolyte (1 M KOH) along with no bubble and O_2 bubbles were observed on the anode, because of lower thermodynamically for EG oxidation than water (Fig. 10e and 10f). On the contrary, H_2 bubbles in both conditions

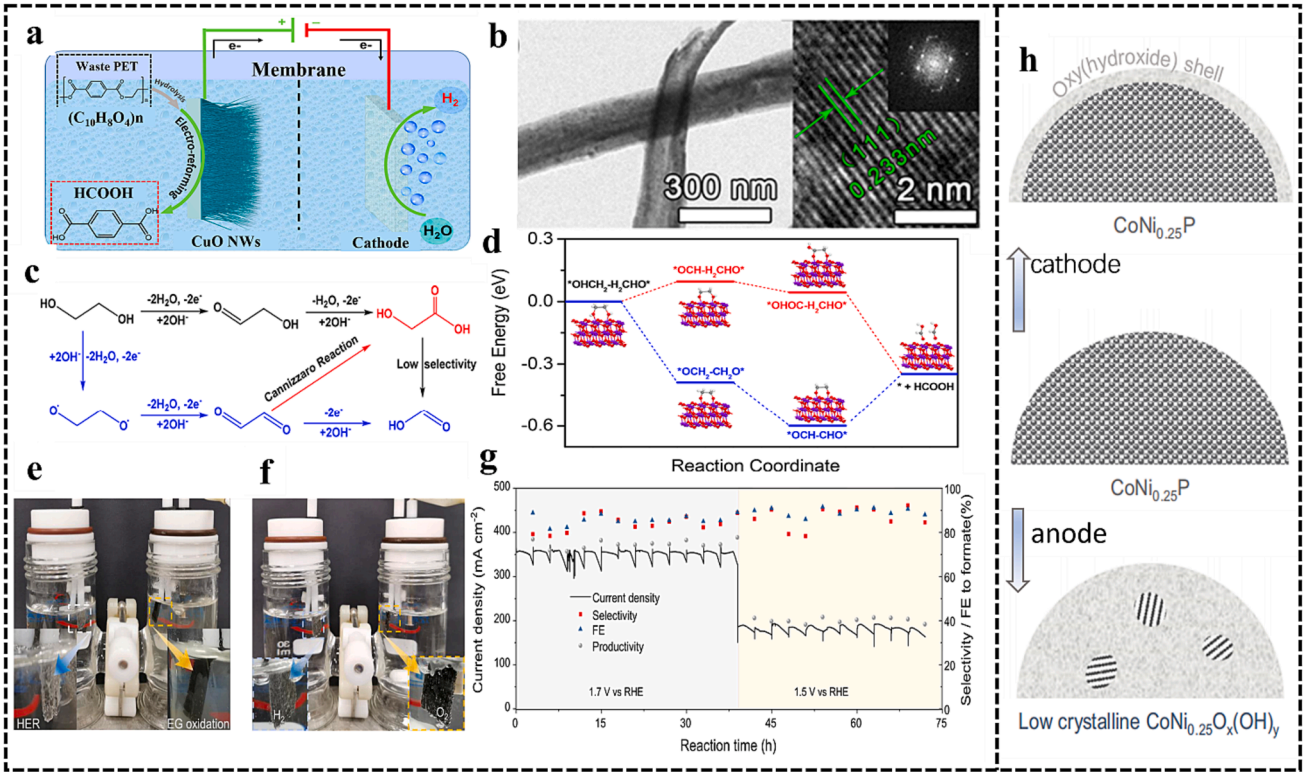

Fig. 10. (a) Electroreforming of PET hydrolysate into HCOOH and H_2. (b) TEM, and HRTEM images of CuO NWs-200 °C. (c) The reaction pathways of EG oxidation in the alkaline electrolyte. (d) The reaction free energy in different pathways during the EG oxidation process [103]. Copyright 2022, The American Chemical Society. Photograph of H-cell configuration for (e) HER//EG oxidation and (f) HER//OER over $CoNi_{0.25}P$/NF at cathode and anode. (g) The stability experiment of $CoNi_{0.25}P$/NF at 1.7 V vs RHE and 1.5 vs RHE for 39 h and 33 h, respectively. (h) The structure of anode and cathode $CoNi_{0.25}P$ after electroreforming of PET hydrolysate. Reproduced with permission [108]. Copyright 2021, Springer Nature.

existed on the cathode surface. When pure glycolic aldehyde and glycolic acid as the substrate, they exhibited higher and lower activities than EG for the formate, respectively, indicating that glycolic aldehyde was more possibly to be the intermediate in the oxidation process of EG. Moreover, 389.2 g formate, 818.5 g PTA, and 16.9 g H_2 could be obtained by electrolysis 1 kg PET after being calculated. In the stability experiment, $CoNi_{0.25}P$/NF at 1.7 V and 1.5 V (vs RHE) both showed high FE (80–95 %) and selectivity (75–95 %) of formate within 39 h and 33 h, severally (Fig. 10g). In addition, the crystalline structure of the $CoNi_{0.25}P$ catalyst was well maintained and only one $CoNi_{0.25}O_x(OH)_y$ shell was formed after HER at the cathode. In contrast, because of the surface reconstruction of $CoNi_{0.25}P$ at the anode, it was oxidized into low-crystalline $CoNi_{0.25}O_x(OH)_y$ (Fig. 10h) conducted to EG oxidation. In a word, this work realizes the conversion of PET into fine chemicals with high efficiency and selectivity, and separates them from reaction solution, successfully. The economic feasibility of the catalytic process is evaluated from a commercial perspective, providing guidance for future research work.

Reisner and coworkers not only converted PE into alkanes by photocatalysis, but also reported the conversion of PE into olefin compounds by electrocatalysis, based on both electrocatalysis and photocatalysis can provide suitable oxidation potential of PE [47]. In the three-electrode system, varying electrode material (carbon Paper, graphite rod or FTO-coated glass sheet) as the working electrode, Ag/AgCl as the reference electrode and Pt as a counter electrode. The activity of ethylene increased with the increase of electrolyte pH values, which was derived from decarboxylation reactions of succinic acid in 0.1 M HNO_3 solution. The faraday efficiency of carbon paper electrode for ethylene generation was 28.6 % at pH 10 and applied potential 2 V vs RHE (Fig. 11a). Besides, a two-electrode electrolyzer was constructed (carbon paper and Pt foil as the working electrode and counter electrode) to assess the conversion rate of succinic acid in methanol and 0.1 M HNO_3 mixed solution (Fig. 11b). The FE of ethylene was 38 % achieved 21.0 μmol $cm_{cat}^{-2}h^{-1}$. Moreover, the PE hydrolysate was also tested in a mixed solution, ethylene and propylene were the main products with FE 4 % and 9 %, achieving 6.0 and 5.0 μmol $cm_{cat}^{-2}h^{-1}$, respectively (Fig. 11c). On the contrary, the FE of H_2 was lower in the mixed solution and higher in the HNO_3 aqueous. This work realizes the conversion of PE into ethylene, which was the molecular monomers in PE synthesis and provides a breakthrough to closed-loop recycling of plastic.

Ma et al. [106] did the electrocatalytic conversion of PET into formic acid coupling with reduction of CO_2 to formic acid (Fig. 11a), so that the faraday efficiency of formic acid was up to 155 %. $NiCo_2O_4$ displayed nanosheet and nanowire spinel structure, while SnO_2 displayed nanosheet structure (Fig. 11b and 11c). Besides, $NiCo_2O_4$/carbon fiber paper (CFP) and SnO_2 carbon cloth (SnO_2/CC) electrodes were investigated in the three-electrode system. $NiCo_2O_4$/CFP electrode showed a lower onset potential in PET hydrolysate compared with pure water (Fig. 11d). On the other hand, SnO_2/CC electrode exhibited excellent activity for the reduction of CO_2 into formic acid in the 1 M $NaHCO_3$ solution with saturated CO_2 (Fig. 11e). Both electrodes exhibited high Faradaic efficiency (FE) for formic acid achieving 90 % and 82 % with the applied

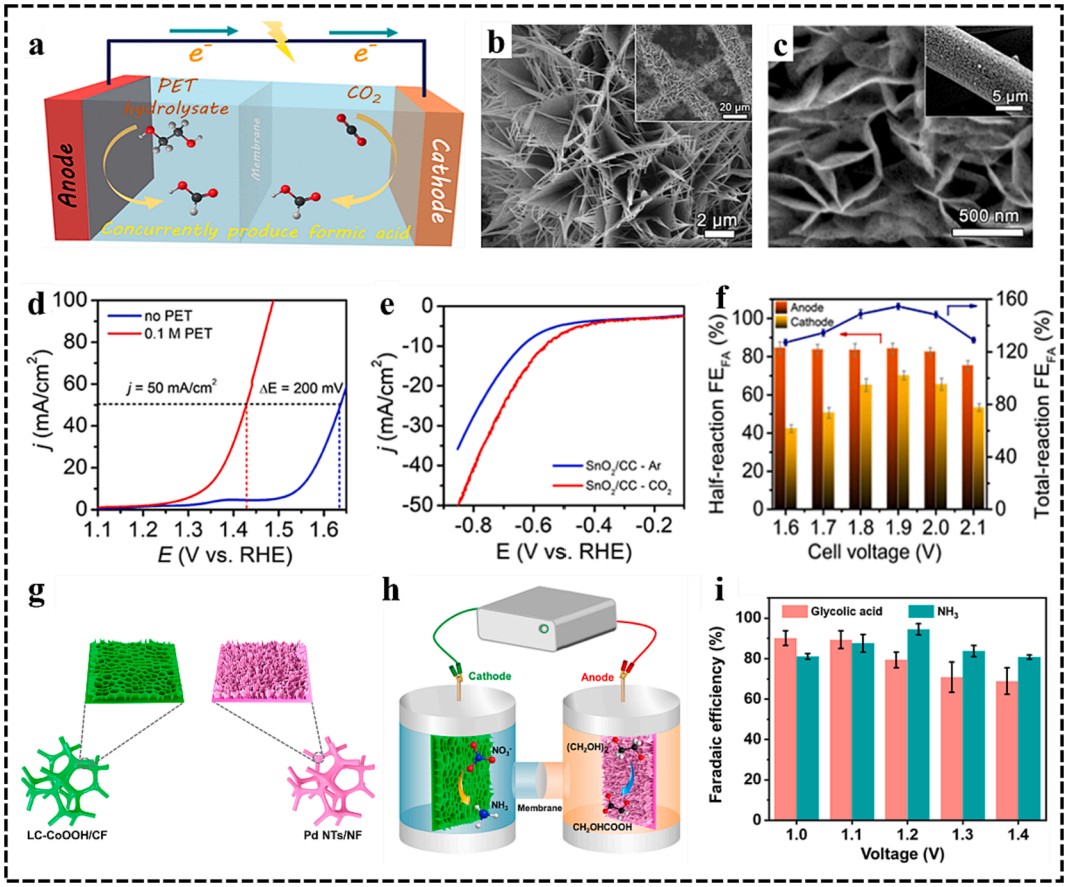

Fig. 11. (a) Electroreforming of PET coupling with reduction of CO_2. SEM images of (b) $NiCo_2O_4$ and (c) SnO_2/CC electrode. (d) LSV curves of electrocatalytic with and without 0.1 M PET in the electrolyte $NiCo_2O_4$/CFP electrode as the anode. (e) LSV curves of electrocatalytic in Ar- or CO_2-saturated 1 M $NaHCO_3$ solutions SnO_2/CC electrode as the cathode. (f) The faradaic efficiencies of PET hydrolysate oxidation and CO_2 reduction for formic acid generation at different applied potentials in the two-electrode system [106]. Copyright 2022, The American Chemical Society. (g) The imagine of LC-CoOOH/CF and Pd NTs/NF electrodes. (h) Schematic diagram of CoOOH/CF||Pd NTs/NF two-electrode system. (i) FE of NH_3 and GA in CoOOH/CF||Pd NTs/NF two-electrode system with various voltages [109]. Copyright 2023, The American Chemical Society.

potential was 1.45 V and − 0.9 V (vs RHE), respectively. Moreover, the two-electrode system was designed for evaluating the total activity to coproduce formic acid. The anode was $NiCo_2O_4$/CFP electrode, which oxidized EG in PET hydrolysate to formic acid with FE of 80 %, meanwhile, the cathode was SnO_2/CC electrode which reduced CO_2 to formic acid with FE of 75 % (Fig. 11f), at an applied potential of 1.9 V (vs RHE). In summary, this work not only realizes the coupling between electroreforming of PET and the reduction of CO_2 to produce formic acid at both electrodes, but also gives the inspiration for generating more valuable chemicals by half-reaction of reduction.

Glycolic acid as a kind of value-added chemicals is utilized to textile and daily chemical industry, expected to reach US $531.5 million by 2027. Given this, Xu et al integrated the plastics oxidation reaction with nitrate reduction reaction by a LC-CoOOH/CF||Pd NTs/NF PEC system [109]. When the applied potential was − 0.25 V (vs RHE), low-crystalline CoOOH (LC-CoOOH/CF) with the rough surface was utilized as cathode which promoted the adsorption of nitrate and provided abundant active sites, leading to a high ammonia faradic efficiency (FE) of 97.38 ± 1.0 % (Fig. 11g). Meanwhile, Pd nanothorns (Pd NTs/NF) with the unique nanothorn morphology was utilized as anode, which facilitated the selective conversion of EG into glycolic acid (GA) with the FE of 87.87 ± 4.0 % at 0.774 V vs RHE. Moreover, the two-electrode coupling system could be conducted at a low applied potential (0.5 V vs RHE) to obtain the co-production, which was much lower than traditional nitrate electrolysis process (1.4 V) (Fig. 11h). Besides, the optimal FE of GA and NH_3 were 90.12 ± 3.6 % and 94.47 ± 2.8 %, and the corresponding applied potential were 1.0 and 1.2 V vs RHE, respectively (Fig. 11i). This study presents a new strategy for plastics reforming through coupling with nitrate reduction to ammonia reaction, further expanding the utilization path-way of plastics waste resource.

4.2. *Photoelectrochemical catalysis for plastics upcycling*

Photoelectrochemical catalysis is the combination of photocatalysis and electrocatalysis, which can maximize the advantages of both technologies. Compared with photocatalysis, the solar energy can be utilized by photoelectrodes to generate photo-generated electrons, improving reaction activity and catalytic efficiency. Compared with electrocatalysis, photoelectrochemical catalysis reactions greatly reduce the injection of external energy, effectively reducing energy consumption. In addition, photoelectrochemical can also apply catalysts that are not suitable for photocatalysis due to band structure mismatch under appropriate applied voltage conditions. Recently, photoelectrochemical catalysis has been widely studied in CO_2 reduction and the valorization of biomass derived compounds [116–118]. In addition, polymer plastics contain abundant organic groups and could also depolymerize into small organic molecules through hydrolysis [119]. Therefore, it is completely feasible to utilize PEC to transform plastics into high-value chemical feedstocks, which provides a broad prospect for the upcycling of plastic waste in real life.

Reisner et al. designed a $Cu_{30}Pd_{70}$|Perovskite|Pt photoelectrochemical (PEC) catalysis device (Fig. 12a) [120]. The introduction of Pd drove the dendritic Cu to take on a flower-like appearance, which was prepared by electrodeposition procedure on the Ni foam (Fig. 12b). Subsequently, the two-electrode PEC system was constructed by Ni foam|$Cu_{30}Pd_{70}$ and perovskite|Pt as the anode and photocathode, respectively, and the perovskite layer was back-illuminated through FTO-glass. When glycerol, ethylene glycol, and glucose as substrates, the production rates of H_2 were 1083,1316, and 1415 μmol H_2 cm^{-2} in 10 h, respectively. On the other hand, the oxidation products were glyceric acid, glycolic acid and gluconic acid, corresponding to 111 ± 28 μmol, 163 ± 45 μmol and 206 ± 46 μmol, respectively and without any applied potential (Fig. 12d and 12e). The high selectivity of the products could be attributed to the high open-circuit voltage (V_{oc}) of 1 V vs. RHE

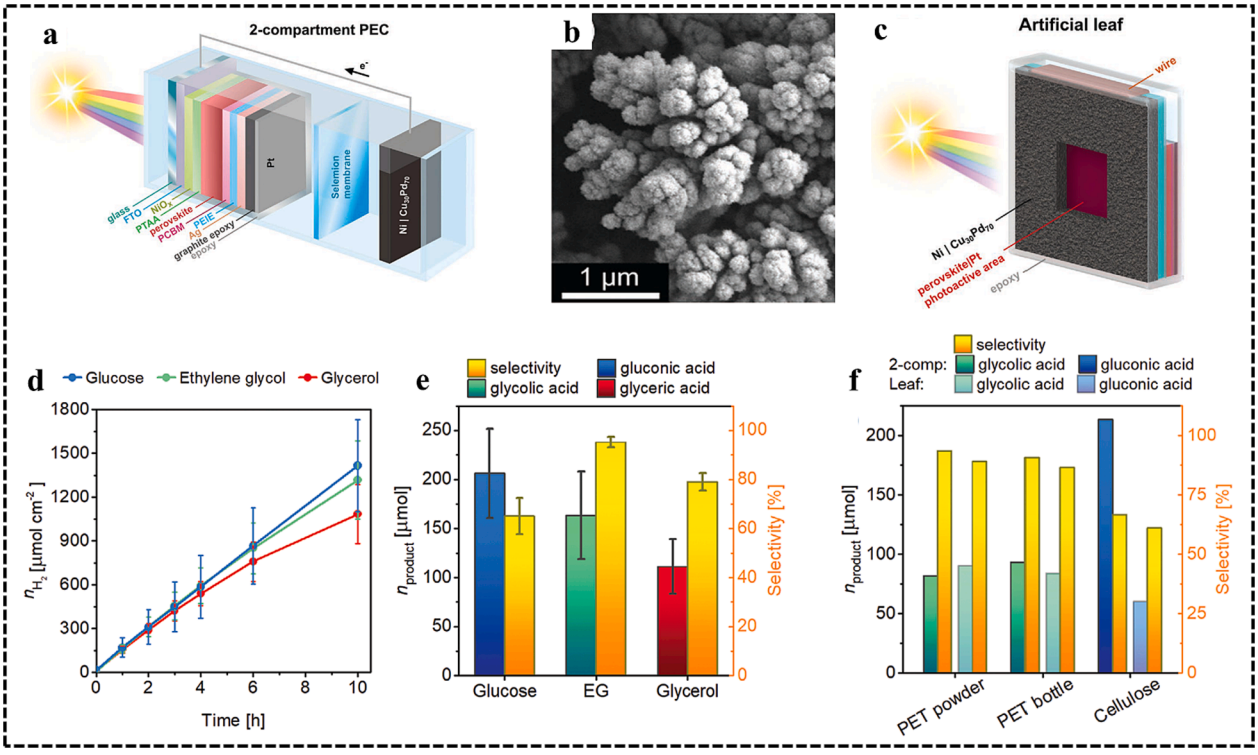

Fig. 12. (a) The $Cu_{30}Pd_{70}$|perovskite|Pt PEC system. (b) SEM image of $Cu_{30}Pd_{70}$. (c) "artificial leaf" configurations. (d) The production yield of H_2 and (e) the amount of oxidation product with different substrates in the PEC system without any applied potential in 10 h. (f) The production yield of oxidation product with different real-world substrates (PET powder, PET bottle, and cellulose) for PEC device in both two-compartment and "artificial leaf" device in 1 M KOH at room temperature without any applied potential for 10 h [120]. Copyright 2021, Wiley.

provided by the perovskite, the overlap potentials for the different substrates and high competition for active sites. Moreover, to explore the real-world convert ability, the PET powder and a real-world commercial PET bottle were reformed by a two-electrode PEC system (Ni foam|$Cu_{30}Pd_{70}$ and perovskite|Pt), the H_2 production was 776 and 748 μmol cm^{-2}, and the selectivity was above 90 %. Furthermore, the PEC system was integrated as a compact system and named "artificial leaf" (Fig. 12c), which could realize redox reactions without applied voltage and wiring. PET powder and PET bottle were then converted into glycolic acid, and at the same time H_2O was reduced to H_2 by artificial leaf without applied voltage (Fig. 12f). In short, the PEC system makes plastic upcycling problems break through the bottleneck, the selectivity of products achieves 60–90 % and the activity are10^2–10^4 times higher than conventional photoreforming systems. Besides, the construction of "artificial leaf" further laying a foundation for the practical application.

Yi's group prepared TiO_2 nanorods photoanode modified by P-Ni alloy thin film (nanoNi-P) and nanoNi-P with carbon nanotubes (CNT-nanoNi-P) cathode to construct nanoTiO_2|nanoNi-P//CNT-nanoNi-P_{op} two-electrode PEC system for converting PET into formic acid and produce H_2, simultaneously (Fig. 13a) [121]. The optimal electrodeposition condition of nanoNi-P was applied current densities (I_{dep}) = −20,000 μA cm^{-2} and $C_{hypophosphite}$ = 0.04 M. On the other hand, in a three-electrodes system, nanoNi-$P_{op(CV)}$ (the optimal nanoNi-P after CV-activation) presented higher activity and Faradaic efficiency (FE) than those for nano$Ni_{(CV)}$, achieved 244.6 μmol $cm^{-2}h^{-1}$ for EG oxidation (Fig. 13b). It is attributed to more β-NiOOH being reserved by the P element as the active species. Moreover, the nanoNi-$P_{op(CV)}$ was integrated onto nanoTiO_2 as the photoanode (C = 0.02C cm^{-2}) showed higher performance than bare nanoTiO_2 photoanode under irradiation (0.5 V vs. RHE). In addition, the two-electrode PEC system was constructed by nanoTiO_2|nanoNi-$P_{op(CV)}$ and CNT-nanoNi-$P_{op(CV)}$ as the photoanode and cathode, respectively. The yield of formate and H_2 were 6.4 μmol and 12.5 μmol, much higher than the PEC system constituted by TiO_2|Pt in 4 h. Finally, the possible mechanism was two hydroxyl groups of EG were oxidized by β-NiOOH to form glyoxal, which was further oxidized into formic acid (Fig. 13c). This study utilizes a photoelectrochemical platform based on nanoNi-$P_{(CV)}$-modified TiO_2 nanorods photoanode and CNT/nanoNi-P cathode to achieve efficient and selective generation of H_2 and formate during the PET reforming process.

Subsequently, Zhao and coworkers designed a PEC system constructed by Fe_2O_3/$Ni(OH)_x$ photoanode, while Ag/AgCl and platinum gauze electrode as the reference electrode and counter electrode, respectively [19]. This PEC system realized the conversion of PET to formic acid and produce H_2 (Fig. 13d). Fe_2O_3/$Ni(OH)_x$ was synthesized by different concentrations of $Ni(NO_3)_2$, and named Fe_2O_3-$_x$Ni. The Fe_2O_3-$_x$Ni photoanode represented more excellent PEC performance than bare Fe_2O_3, where Fe_2O_3-10Ni was the optimal. Because of the competition between the oxidation of EG and water splitting at high potentials, the Fe_2O_3-10Ni electrode exhibited an FE of about 100 % at a

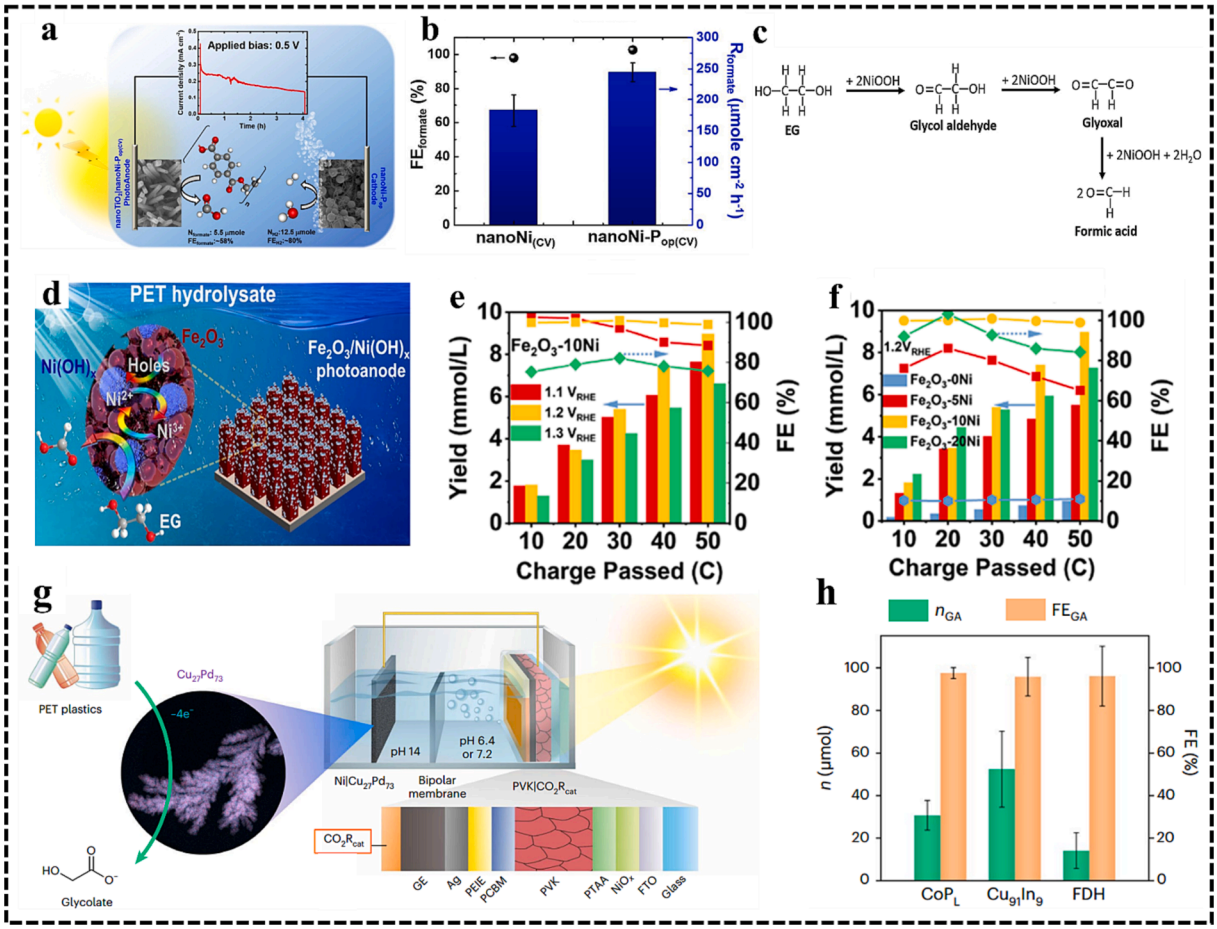

Fig. 13. (a) The nanoTiO_2|nanoNi-P_{op}(CV)//CNT-nanoNi-P_{op} two-electrode PEC system for reforming PET hydrolysate into formic acid and H_2. (b) The production rate and FE of formic acid over nanoNi-$P_{op(CV)}$ and nanoNi-$P_{(CV)}$ at 1.5 V vs. RHE for EG oxidation in KOH solution. (c)The reaction mechanism of EG oxidation over nanoNi-$P_{op(CV)}$ photoanode [121]. Copyright 2022, Elsevier. (d) The upcycling of PET over Fe_2O_3/$Ni(OH)_x$ photoanode. (e) The formic acid yield and FE over Fe_2O_3-10Ni at different applied bias and (f) different Ni loading of Fe_2O_3-xNi photoelectrodes at the applied bias of 1.2 V_{RHE} [19]. Copyright 2022, the American Chemical Society. (g) Schematic diagram of $Cu_{27}Pd_{73}$||PVK|CO_2R_{cat} PEC system. (h) The amount and corresponding FEs of oxidation product formed at the anode with the pretreated PET after a 10 h PEC reforming without applied voltage [33]. Copyright 2022, Springer Nature.

lower potential, and with the increase of potential, the FE of formic acid decreased to less than 80 % (Fig. 13e). Moreover, at the potential of 1.2 V_{RHE}, the FE of Fe_2O_3-10Ni and Fe_2O_3-20Ni photoanodes were higher than Fe_2O_3-5Ni and Fe_2O_3-0Ni (Fig. 13f). Furthermore, Fe_2O_3-10Ni was then studied in the higher concentration of PET hydrolysate, and retained photoelectrocatalytic performance in KOH electrolyte. Finally, the possible working mechanism of $Fe_2O_3/Ni(OH)_x$ photoanode was proposed, with the Ni^{2+} being oxidized into Ni^{3+} by the photogenerated holes from the Fe_2O_3. The Ni^{3+} centers promptly react with EG to yield formate. This work investigates the mechanism based on Ni^{2+}/Ni^{3+} redox couple and suggests that the introduction of $Ni(OH)_x$ cocatalyst can effectively regulate the oxidation ability of the photogenerated holes, thereby improving the selectivity towards the desired formic acid products during the photoelectrochemical catalytic process of PET waste.

Besides H_2, other valuable chemicals, such as the products of CO_2 reduction and N_2-based synthesis of ammonia can also be achieved through reduction reaction. Taking the advantages separating oxidation and reduction processes with minimized crossover reactions of photoelectrochemical catalysis, Reisner and co-workers realized the plastics oxidation coupling with the CO_2 reduction by a $Cu_{27}Pd_{73}||PVK|CO_2R_{cat}$ (CO_2R_{cat}: CO_2R catalysts) PEC systems (Fig. 13g) [33]. This PEC system could selectively convert the pretreated PET into glycolic acid (GA) in different pH without applied voltage. Meanwhile, when the CO_2R_{cat} photocathode were lipophilic, alkyl-functionalized cobalt porphyrin (CoP_L), copper–indium ($Cu_{91}In_9$) and formate dehydrogenase from *Desulfovibrio vulgaris* Hildenborough (FDH), the main products were CO, syngas and formate, respectively. PEC analysis showed that the working potentials of CoP_L, $Cu_{91}In_9$ and FDH were –0.7 V, –0.7 V and –0.8 V versus RHE (AM 1.5G 0.5 M $KHCO_3$ electrolyte) and exhibited the Faradaic efficiency (FE) of corresponding products were 85 ± 2 %, 94 % (FE_{CO} = 48 ± 8 % and FE_{H2} = 46 ± 4 %) and 96 ± 2 %, respectively. In solar-driven PEC experiments, $Cu_{27}Pd_{73}$ anode and $PVK|CO_2R_{cat}$ photocathodes were separated by a bipolar membrane, the anolyte and photocathode consisted of 1 M aqueous KOH and 0.5 M aqueous $KHCO_3$ (CO_2-saturated electrolyte for FDH). As a result, the CO, syngas (CO and H_2) and formate were produced from the $PVK|CO_2R_{cat}$ (CoP_L, $Cu_{91}In_9$ and FDH) photocathodes, and their evolution rates were 263 ± 99, 452 (CO: 212 ± 148|H_2: 240 ± 75) and 121 ± 87 μmol cm^{-2}, respectively. Meanwhile, the GA was produced from the $Cu_{27}Pd_{73}$ anode with yields of 31 ± 7, 52 ± 18 and 14 ± 8 μmol after 10 h in the three different cases (Fig. 13i). In short, this work integrates single-light-absorber $Cu_{27}Pd_{73}||PVK|CO_2R_{cat}$ PEC device with effort to couple CO_2 reduction with plastics reforming and presents a unique demonstration for sustainable commercial implementation.

4.3. Solar thermal electrochemical conversion

Traditional pyrolysis of plastics has been broadly studied in the past decades [122,123]. Generally, pyrolysis of plastics demands a temperature of about 500 ℃ even higher temperature in the range of 700 ℃–900 ℃ to improve productivity [124]. But higher temperature means more energy requirements, which is not economical and environmentally friendly. The solar thermal electrochemical process (STEP) has captured the researcher's attention from 2009 [125–128]. In a STEP system, the solar energy can be converted into electric and heat energy, thermal energy has the potential to effectively decrease the energy required for the endothermic process of electrolysis, allowing it to surpass the activation energy necessary for the redox reaction. This greatly promotes the enhancement of solar utilization and conversion efficiency of plastics waste [23]. Besides, solar energy is the sole power source in the STEP system with no necessary for any external energy source. Therefore, it is a clean and sustainable strategy to make use of STEP to upcycle waste plastics [129,130].

Wang et al. realized the conversion of polypropylene (PP) to H_2, CH_4, C_2H_6, C_3H_4, and C_5H_{12} through the STEP system, constructed by them. In this system, a solar thermal collector and the photovoltaic panel provided heat and electricity for the reaction process (Fig. 14a), respectively [23]. At 350 °C to 400 °C, the total conversion rate of PP by STEP not only increased with the rise of temperature, but also was higher than the conversion rate of pure heat at the same temperature, indicating that electric field played an important role in STEP system. Meanwhile, the effect of electrolysis current exhibited the same rule for the STEP transformation of PP, the total conversion rate could achieve 52.02 % when the current was 400 mA at 400 °C, while the conversion rate was 42.08 % corresponding to 0 mA at 400 °C, in an hour. The other significant difference between STEP and pyrolysis was the productivity of H_2, the yield of STEP H_2 was 10.3 times that of pure pyrolysis and 2.9 times that of pure electrolysis (Fig. 14b). Moreover, the STEP system was also studied outdoors for exploring its stability. In the optimal, the conversion of PP reached 66.64 % exhibiting excellent conversion ratio and stability, meanwhile, the conversion just was 26.37 % of the pyrolysis. In this work, the coupling between the solar concentrators and solar cell packs technology is achieved to the convert the plastics waste efficiently. Moreover, the STEP is completely driven by sustainable solar energy and the equipment of STEP system is not high. In short, the STEP system lays the foundation for industrialization of plastic upcycling.

5. Conclusion and outlook

The massive generation of plastic waste has resulted in serious environmental and ecological crisis, yet plastics can be regarded as raw carbon materials to produce value-added chemicals by catalytic methods. This mini review summaries the progress for the conversion of plastic into fuels, fine chemicals and materials, with focus on photocatalysis, electrocatalysis, photoelectrochemical (PEC) catalysis and solar thermal electrochemical process (STEP) as well as the pretreatment method of various plastics. Compared with the traditional treatment of plastics, the upcycling by photo- and electrochemical processes produce higher add-value products. Moreover, the photo- and electrochemical processes conduct in ambient condition, which are more environmentally friendly and sustainable compare with the thermocatalysis under harsh conditions. In short, these technologies based on clean energy from solar and electricity energy may attract more attention in the future owing to environmental sustainability.

However, these technologies for plastic upcycling are still in the early stages of development, and there is still a huge space to improve the efficiency, product selectivity and stability for practical production and real applications. Finally, we propose the worth research directions from perspective of catalytic in the field of plastic upcycling:

1) Catalyst improvements: Catalysts with high efficiency, low cost, easy synthesis and high selectivity are the necessary conditions for plastics waste upcycling. Till now, few catalysts have been utilized to explore plastics upcycling, suggesting that more catalysts should be studied in this process. Taking photocatalytic materials as example, attention should be paid to the development of narrow band gap semiconductors, which can absorb the solar light as much as possible, since plastic conversion is much more thermodynamically favorable than water splitting. Additionally, the study of composite catalysts should also be further emphasized, due to the performance of a single photocatalyst is often limited. Consequently, combining different catalysts are advantageous in overcoming the activity bottleneck and leveraging the benefits of multiple catalytic materials.

2) Reaction mechanism: Exploring the mechanism of plastics conversion is important to adjust and improve the utilized catalyst, further understanding the chemical changes on catalyst' surface, thereby enhancing the activity and selectivity towards a target product. Advanced characterization methods and theoretical calculations could be helpful to get an insight about the reaction mechanism of plastics conversion, and break the bottlenecks which limit the activity or selectivity of the used catalytic materials, further promoting the industrialization of plastics upcycling. For example, in-situ FTIR analysis has

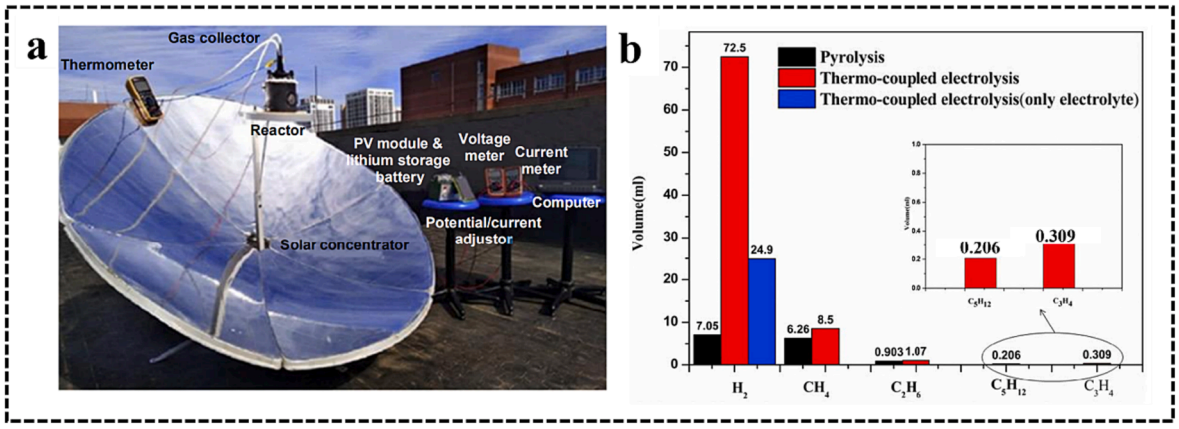

Fig. 14. (a) The device of the outdoor experiments. (b) The production yield (H_2, CH_4 and C_2H_6) of pyrolysis, electrolysis and STEP process for reforming PP hydrolysate [23]. Copyright 2020, Elsevier.

been employed to monitor reactive intermediates in plastics upcycling. However, its effectiveness is still far from satisfactory. Given this, it is vital to combine in-situ mass spectrometry and isotope-labeling experiments to elucidate the reaction pathway, which is mutually corroborating with in-situ FTIR analysis, further explaining the evolution of intermediates during plastics upcycling. Based on these advanced characterization analyses, we could design controlled experiment to find the main drawbacks during plastic conversion, as well as design more suitable catalysts with enhanced activity and selectivity towards a target product. On the other hand, both thermodynamic and kinetic studies are significantly important during plastic conversion and can be effectively explored through theoretical studies. In particular, for photocatalysis and electrocatalysis of plastics initiated by charge carriers, redox potential and quantity of charge carriers should be appropriately adjusted to satisfy the requirement of theoretical thermodynamic potentials for promoting the activity and selectivity of catalytic materials in plastics conversion. In addition, the pH of the solution and the rate-limiting step are key kinetic parameters, which should also be explored by the theoretical studies to pursue optimal catalytic conditions.

3) Reaction coupling: Upcycling of plastics consist of oxidation and reduction half-reactions, in which the reduction half-reaction is mainly to reduce water to H_2. However, it has the potential to generate more valuable chemicals, such as CO_2 reduction and N_2-based synthesis of ammonia, but limited work has been done in this area. Additionally, it is worthy to note that the use of coupling between existing technologies should be considered, since coupling technologies can often produce a synergistic effect, such as photoelectrochemical and photo-thermal electrochemical processes.

4) Design of reaction equipment: Up to now, plastics upcycling by clean energy technologies is mostly carried out in the laboratory trial stage, and it is necessary to design large-scale reaction equipment for future practical applications. Moreover, establishing a mobile phase reaction equipment to increase the contact between plastics and catalysts can better promote catalytic performance for photocatalysis and electrocatalysis upcycling of plastics. As for plastic photocatalysis, sufficient light source is a necessary condition, thus the collector (such as a convex lens) can be utilized to increase the light intensity in the site where the catalyst is located, further improving catalytic efficiency. Besides, the fixation of photocatalysts (frosted glass) is also crucial, which is beneficial for recycling and environmental protection. With the development of photovoltaic technology, electrocatalysis upcycling of plastics can be combined with distributed photovoltaic technology to meet its electricity demand.

CRediT authorship contribution statement

Xinxin Liang: Writing – original draft, Writing – review & editing. **Ximing Li:** Writing – review & editing. **Qibing Dong:** Formal analysis. **Ting Gao:** Resources. **Mengxin Cao:** Validation. **Ke Zhao:** Software. **Eric Lichtfouse:** Writing – review & editing. **Antonio Otavio T. Patrocinio:** Writing – review & editing. **Chuanyi Wang:** Funding acquisition, Validation, Writing – review & editing.

Declaration of competing interest

The authors declare that they have no known competing financial interests or personal relationships that could have appeared to influence the work reported in this paper.

Data availability

The authors do not have permission to share data.

Acknowledgements

This work was supported by the National Natural Science Foundation of China (52161145409, 21976116), SAFEA of China ("Belt and Road" Innovative Talent Exchange Foreign Expert Project # 2023041004L) (High-end Foreign Expert Project # G2023041021L), and Alexander-von-Humboldt Foundation of Germany (Group-Linkage Program). AOTP is thankful to the Phosagro/IUPAC/UNESCO research program in green chemistry.

References

[1] X. Jiao, K. Zheng, Z. Hu, S. Zhu, Y. Sun, Y. Xie, Conversion of waste plastics into value-added carbonaceous fuels under mild conditions, Adv. Mater. 33 (2021) 2005192.
[2] K. Tang, A. Zhang, T. Ge, X. Liu, X. Tang, Y. Li, Research progress on modification of phenolic resin, Mater. Today Commun. 26 (2021) 101879.
[3] R.J. Conk, S. Hanna, J.X. Shi, J. Yang, N.R. Ciccia, L. Qi, B.J. Bloomer, S. Heuvel, T. Wills, J. Su, A.T. Bell, J.F. Hartwig, Catalytic deconstruction of waste polyethylene with ethylene to form propylene, Science 377 (2022) 1561–1566.
[4] L.D. Ellis, N.A. Rorrer, K.P. Sullivan, M. Otto, J.E. McGeehan, Y. Román-Leshkov, N. Wierckx, G.T. Beckham, Chemical and biological catalysis for plastics recycling and upcycling, Nat. Catal. 4 (2021) 539–556.
[5] M. Bergmann, F. Collard, J. Fabres, G.W. Gabrielsen, J.F. Provencher, C. M. Rochman, E. van Sebille, M.B. Tekman, Plastic pollution in the Arctic, Nat. Rev. Earth. Env. 3 (2022) 323–337.
[6] K. Zheng, Y. Wu, Z. Hu, S. Wang, X. Jiao, J. Zhu, Y. Sun, Y. Xie, Progress and perspective for conversion of plastic wastes into valuable chemicals, Chem. Soc. Rev. 52 (2023) 8–29.
[7] M. MacLeod, H.P.H. Arp, M.B. Tekman, A. Jahnke, The global threat from plastic pollution, Science 373 (2021) 61–65.
[8] A. Turner, Paint particles in the marine environment: an overlooked component of microplastics, Water Res. X 12 (2021) 100110.
[9] Z. Ouyang, Y. Yang, C. Zhang, S. Zhu, L. Qin, W. Wang, D. He, Y. Zhou, H. Luo, F. Qin, Recent advances in photocatalytic degradation of plastics and plastic-derived chemicals, J. Mater. Chem. A 9 (2021) 13402–13441.

[10] I. Vollmer, M.J.F. Jenks, M.C.P. Roelands, R.J. White, T. van Harmelen, P. de Wild, G.P. van der Laan, F. Meirer, J.T.F. Keurentjes, B.M. Weckhuysen, Beyond mechanical recycling: giving new life to plastic waste, Angew. Chem. Int. Edit. 59 (2020) 15402–15423.

[11] X. Chen, Y. Wang, L. Zhang, Recent progress in the chemical upcycling of plastic wastes, ChemSusChem 14 (2021) 4137–4151.

[12] T. Thiounn, R.C. Smith, Advances and approaches for chemical recycling of plastic waste, J. Polym. Sci. 58 (2020) 1347–1364.

[13] H. Zhou, Y. Wang, Y. Ren, Z. Li, X. Kong, M. Shao, H. Duan, Plastic waste valorization by leveraging multidisciplinary catalytic technologies, ACS Catal. 12 (2022) 9307–9324.

[14] D.J. Lipomi, Video for active and remote learning, Trends Chem. 2 (2020) 483–485.

[15] V.K. Soni, G. Singh, B.K. Vijayan, A. Chopra, G.S. Kapur, S.S.V. Ramakumar, Thermochemical recycling of waste plastics by pyrolysis: a review, Energ Fuel. 35 (2021) 12763–12808.

[16] R.-X. Yang, K. Jan, C.-T. Chen, W.-T. Chen, K.C.W. Wu, Thermochemical conversion of plastic waste into fuels, chemicals, and value-added materials: a critical review and outlooks, Chem. Sus. Chem. 15 (2022) e202200171.

[17] M. Du, Y. Zhang, S. Kang, C. Xu, Y. Ma, L. Cai, Y. Zhu, Y. Chai, B. Qiu, Electrochemical production of glycolate fuelled by polyethylene terephthalate plastics with improved techno-economics, Small 19 (2023) 2303693.

[18] S. Chu, B. Zhang, X. Zhao, H.S. Soo, F. Wang, R. Xiao, H. Zhang, Photocatalytic conversion of plastic waste: from photodegradation to photosynthesis, Adv. Energy Mater. 12 (2022) 2200435.

[19] X. Li, J. Wang, T. Zhang, T. Wang, Y. Zhao, Photoelectrochemical catalysis of waste polyethylene terephthalate plastic to coproduce formic acid and hydrogen, Acs Sustain. Chem. Eng. 10 (2022) 9546–9552.

[20] C. Li, X.Y. Kong, M. Lyu, X.T. Tay, M. Đokić, K.F. Chin, C.T. Yang, E.K.X. Lee, J. Zhang, C.Y. Tham, W.X. Chan, W.J. Lee, T.T. Lim, A. Goto, M.B. Sullivan, H. S. Soo, Upcycling of non-biodegradable plastics by base metal photocatalysis, Chem 9 (2023) 2683–2700.

[21] J. Wang, X. Li, T. Zhang, X. Qian, T. Wang, Y. Zhao, Rational design of photo−/electro−catalytic systems for the transformation of plastic wastes, Appl. Catal. B-Environ. 332 (2023) 122744.

[22] M.A. Marwat, M. Humayun, M.W. Afridi, H. Zhang, M.R. Abdul Karim, M. Ashtar, M. Usman, S. Waqar, H. Ullah, C. Wang, W. Luo, Advanced catalysts for photoelectrochemical water splitting, Acs Appl Energ. Mater. 4 (2021) 12007–12031.

[23] T. Jiang, X. Zhao, D. Gu, C. Yan, H. Jiang, H. Wu, B. Wang, X. Wang, STEP polymer degradation: solar thermo-coupled electrochemical depolymerization of plastics to generate useful fuel plus abundant hydrogen, Sol. Energ. Mat. Sol. c. 204 (2020) 110208.

[24] J. Lee, J. Yang, J.H. Moon, Solar cell-powered electrochemical methane-to-methanol conversion with CuO/CeO_2 catalysts, Acs Energy Lett. 6 (2021) 893–899.

[25] B. Zhang, H. Zhang, Y. Pan, J. Shao, X. Wang, Y. Jiang, X. Xu, S. Chu, Photoelectrochemical conversion of plastic waste into high-value chemicals coupling hydrogen production, Chem. Eng. J. 462 (2023) 142247.

[26] T. Uekert, M.F. Kuehnel, D.W. Wakerley, E. Reisner, Plastic waste as a feedstock for solar-driven H2 generation, Energ. Environ. Sci. 11 (2018) 2853–2857.

[27] M. Du, M. Xing, W. Yuan, L. Zhang, T. Sun, T. Sheng, C. Zhou, B. Qiu, Upgrading polyethylene terephthalate plastic into commodity chemicals paired with hydrogen evolution over a partially oxidized $CuIn_5S_8$ nanosheet photocatalyst, Green Chem. 25 (2023) 9818–9825.

[28] X. Jiao, K. Zheng, Q. Chen, X. Li, Y. Li, W. Shao, J. Xu, J. Zhu, Y. Pan, Y. Sun, Y. Xie, Photocatalytic conversion of waste plastics into C2 fuels under simulated natural environment conditions, Angew. Chem. Int. Edit. 59 (2020) 15497–15501.

[29] T. Uekert, H. Kasap, E. Reisner, Photoreforming of nonrecyclable plastic waste over a carbon nitride/nickel phosphide catalyst, J. Am. Chem. Soc. 141 (2019) 15201–15210.

[30] S. Kang, T. Sun, Y. Ma, M. Du, M. Gong, C. Zhou, Y. Chai, B. Qiu, Artificial photosynthesis bringing new vigor into plastic wastes, SmartMat 4 (2023) e1202.

[31] Y. Ma, Y. Zhang, W. Yuan, M. Du, S. Kang, B. Qiu, Electroreforming injects a new life into solid waste, EES Catal. 1 (2023) 892–920.

[32] M. Du, Y. Zhang, S. Kang, X. Guo, Y. Ma, M. Xing, Y. Zhu, Y. Chai, B. Qiu, Trash to treasure: photoreforming of plastic waste into commodity chemicals and hydrogen over MoS_2-tipped CdS nanorods, ACS Catal. 12 (2022) 12823–12832.

[33] S. Bhattacharjee, M. Rahaman, V. Andrei, M. Miller, S. Rodríguez-Jiménez, E. Lam, C. Pornrungroj, E. Reisner, Photoelectrochemical CO_2-to-fuel conversion with simultaneous plastic reforming, Nat. Synth. 2 (2023) 182–192.

[34] A. Kamimura, S. Yamamoto, An efficient method to depolymerize polyamide plastics: a new use of ionic liquids, Org. Lett. 9 (2007) 2533–2535.

[35] H.F. Son, I.J. Cho, S. Joo, H. Seo, H.-Y. Sagong, S.Y. Choi, S.Y. Lee, K.-J. Kim, Rational protein engineering of thermo-stable petase from ideonella sakaiensis for highly efficient pet degradation, ACS Catal. 9 (2019) 3519–3526.

[36] R. Cao, D. Xiao, M. Wang, Y. Gao, D. Ma, Solar-driven photocatalysis for recycling and upcycling plastics, Appl. Catal. B-Environ. 341 (2024) 123357.

[37] X. Jiao, Z. Hu, Y. Wu, K. Zheng, L. Li, S. Zhu, W. Shao, J. Zhu, Y. Pan, Y. Sun, Photoconverting polyethylene terephthalate into exclusive carbon dioxide by heterostructured NiO/Fe_2O_3 nanosheets under mild conditions, Sci. China. Mater. 65 (2022) 985–991.

[38] J. Shang, M. Chai, Y. Zhu, Photocatalytic degradation of polystyrene plastic under fluorescent light, Environ. Sci. Technol. 37 (2003) 4494–4499.

[39] X. Zhao, B. Boruah, K.F. Chin, M. Đokić, J.M. Modak, H.S. Soo, Upcycling to sustainably reuse plastics, Adv. Mater. 34 (2022) 2100843.

[40] M. Chu, Y. Liu, X. Lou, Q. Zhang, J. Chen, Rational design of chemical catalysis for plastic recycling, ACS Catal. 12 (2022) 4659–4679.

[41] P. Sivaguru, Z. Wang, G. Zanoni, X. Bi, Cleavage of carbon–carbon bonds by radical reactions, Chem. Soc. Rev. 48 (2019) 2615–2656.

[42] S.E. Lewis, B.E. Wilhelmy, F.A. Leibfarth, Organocatalytic C-H fluoroalkylation of commodity polymers, Poly. Chem. 11 (2020) 4914–4919.

[43] J. Xu, X. Jiao, K. Zheng, W. Shao, S. Zhu, X. Li, J. Zhu, Y. Pan, Y. Sun, Y., Xie, Plastics-to-syngas photocatalysed by $Co–Ga_2O_3$ nanosheets, Natl. Sci. Rev. 9 (2022) nwac011.

[44] J. Qin, Y. Dou, F. Wu, Y. Yao, H.R. Andersen, C. Hélix-Nielsen, S.Y. Lim, W. Zhang, In-situ formation of Ag2O in metal-organic framework for light-driven upcycling of microplastics coupled with hydrogen production, Appl. Catal. B-Environ. 319 (2022) 121940.

[45] B. Cao, S. Wan, Y. Wang, H. Guo, M. Ou, Q. Zhong, Highly-efficient visible-light-driven photocatalytic H2 evolution integrated with microplastic degradation over MXene/ZnxCd1-xS photocatalyst, J. Colloid Interf. Sci. 605 (2022) 311–319.

[46] T. Kawai, T. Sakata, Photocatalytic hydrogen production from water by the decomposition of poly-vinylchloride, protein, algae, dead insects, and excrement, Chem. Lett. 10 (1981) 81–84.

[47] C.M. Pichler, S. Bhattacharjee, M. Rahaman, T. Uekert, E. Reisner, Conversion of polyethylene waste into gaseous hydrocarbons via integrated tandem chemical–photo/electrocatalytic processes, ACS Catal. 11 (2021) 9159–9167.

[48] C. Xing, G. Yu, J. Zhou, Q. Liu, T. Chen, H. Liu, X. Li, Solar energy-driven upcycling of plastic waste on direct Z-scheme heterostructure of V-substituted phosphomolybdic acid/g-C_3N_4 nanosheets, Appl. Catal. B-Environ. 315 (2022) 121496.

[49] J. Ran, J. Zhang, J. Yu, M. Jaroniec, S.Z. Qiao, Earth-abundant cocatalysts for semiconductor-based photocatalytic water splitting, Chem. Soc. Rev. 43 (2014) 7787–7812.

[50] B.-J. Ng, L.K. Putri, X.Y. Kong, Y.W. Teh, P. Pasbakhsh, S.-P. Chai, Z-scheme photocatalytic systems for solar water splitting, Adv. Sci. 7 (2020) 1903171.

[51] J. Liu, Y. Li, X. Zhou, H. Jiang, H.G. Yang, C. Li, Positively charged Pt-based cocatalysts: an orientation for achieving efficient photocatalytic water splitting, J. Mater. Chem. A 8 (2020) 17–26.

[52] R. Marschall, L. Wang, Non-metal doping of transition metal oxides for visible-light photocatalysis, Catal. Today 225 (2014) 111–135.

[53] Y.-X. Pan, Z.-Q. Sun, H.-P. Cong, Y.-L. Men, S. Xin, J. Song, S.-H. Yu, Photocatalytic CO_2 reduction highly enhanced by oxygen vacancies on Pt-nanoparticle-dispersed gallium oxide, Nano Res. 9 (2016) 1689–1700.

[54] G.C. de Assis, E. Skovroinski, V.D. Leite, M.O. Rodrigues, A. Galembeck, M.C. F. Alves, J. Eastoe, R.J. de Oliveira, Conversion of "Waste Plastic" into photocatalytic nanofoams for environmental remediation, ACS Appl. Mater. Inter. 10 (2018) 8077–8085.

[55] A.G. Naikwade, M.B. Jagadale, D.P. Kale, A.D. Gophane, K.M. Garadkar, G. S. Rashinkar, Photocatalytic degradation of methyl orange by magnetically retrievable supported ionic liquid phase photocatalyst, ACS Omega 5 (2020) 131–144.

[56] Y. Bai, K. Hippalgaonkar, R.S. Sprick, Organic materials as photocatalysts for water splitting, J. Mater. Chem. A 9 (2021) 16222–16232.

[57] S. Kikkawa, K. Teramura, H. Asakura, S. Hosokawa, T. Tanaka, Development of Rh-Doped Ga_2O_3 photocatalysts for reduction of CO_2 by H_2O as an electron donor at a more than 300 nm wavelength, J. Phys. Chem. C 122 (2018) 21132–21139.

[58] C. Zhou, S. Wang, Z. Zhao, Z. Shi, S. Yan, Z. Zou, A facet-dependent schottky-junction electron shuttle in a BiVO4{010}–Au–Cu2O Z-scheme photocatalyst for efficient charge separation, Adv. Funct. Mater. 28 (2018) 1801214.

[59] X. Yu, B. Kim, Y.K. Kim, Highly enhanced photoactivity of anatase TiO_2 nanocrystals by controlled hydrogenation-induced surface defects, ACS Catal. 3 (2013) 2479–2486.

[60] T. Uekert, M.A. Bajada, T. Schubert, C.M. Pichler, E. Reisner, Scalable photocatalyst panels for photoreforming of plastic, biomass and mixed waste in flow, ChemSusChem 14 (2021) 4190–4197.

[61] Y. Gu, Y.-N. Wu, L. Li, W. Chen, F. Li, S. Kitagawa, Controllable modular growth of hierarchical MOF-on-MOF architectures, Angew. Chem. Int. Edit. 56 (2017) 15658–15662.

[62] S. Cao, B. Shen, T. Tong, J. Fu, J. Yu, 2D/2D heterojunction of ultrathin MXene/Bi_2WO_6 nanosheets for improved photocatalytic CO_2 reduction, Adv. Funct. Mater. 28 (2018) 1800136.

[63] X. Li, Q. Dong, Q. Tian, A. Sial, H. Wang, H. Wen, B. Pan, K. Zhang, J. Qin, C. Wang, Recent advance in metal- and covalent-organic framework-based photocatalysis for hydrogen evolution, Mater. Today Chem. 26 (2022) 101037.

[64] X. Liang, J. Zhao, T. Wang, Z. Zhang, M. Qu, C. Wang, Constructing a Z-scheme heterojunction photocatalyst of $GaPO_4/\alpha$-MoC/Ga_2O_3 without mingling type-II heterojunction for CO_2 reduction to CO, Acs Appl. Mater. Inter. 13 (2021) 33034–33044.

[65] L. Yuan, L. Buzoglu Kurnaz, C. Tang, alternative plastics, Nature Sustain. 4 (2021) 837–838.

[66] Plastic upcycling, Nat. Catal. 2 (2019) 945-946.

[67] T. Li, A. Vijeta, C. Casadevall, A.S. Gentleman, T. Euser, E. Reisner, Bridging plastic recycling and organic catalysis: photocatalytic deconstruction of polystyrene via a C-H oxidation pathway, Acs Catal. 12 (2022) 8155–8163.

[68] Plastics give and plastics take, Nat. Rev. Mater. 7 (2022) 67-67.

[69] X. Zhao, M. Korey, K. Li, K. Copenhaver, H. Tekinalp, S. Celik, K. Kalaitzidou, R. Ruan, A.J. Ragauskas, S. Ozcan, Plastic waste upcycling toward a circular economy, Chem. Eng. J. 428 (2022) 131928.

[70] O. Horodytska, D. Kiritsis, A. Fullana, Upcycling of printed plastic films: LCA analysis and effects on the circular economy, J. Clean Prod. 268 (2020) 122138.
[71] Q. Yue, L. Luo, Turning trash into treasure: metal-free upcycling of polystyrene plastic waste to aromatics, Chem 8 (2022) 2326–2329.
[72] B. Thijs, J. Rongé, J.A. Martens, Matching emerging formic acid synthesis processes with application requirements, Green Chem. 24 (2022) 2287–2295.
[73] N.V. Rees, R.G. Compton, Sustainable energy: a review of formic acid electrochemical fuel cells, J. Solid. State Electr. 15 (2011) 2095–2100.
[74] H. Yi, L. Qin, D. Huang, G. Zeng, C. Lai, X. Liu, B. Li, H. Wang, C. Zhou, F. Huang, S. Liu, X. Guo, Nano-structured bismuth tungstate with controlled morphology: Fabrication, modification, environmental application and mechanism insight, Chem. Eng. J. 358 (2019) 480–496.
[75] N. Yahya, F. Aziz, A. Jamaludin, A. Aizat, M.A. Mutalib, J. Jaafar, W.J. Lau, N. Yusof, W.N.W. Salleh, A.F. Ismail, Effects of the citric acid addition on the morphology, surface area, and photocatalytic activity of $LaFeO_3$ nanoparticles prepared by glucose-based gel combustion methods, Ind. Eng. Chem. Res. 58 (2019) 609–617.
[76] S. Lotfi, M.E. Ouardi, H.A. Ahsaine, A. Assani, Recent progress on the synthesis, morphology and photocatalytic dye degradation of $BiVO_4$ photocatalysts: a review, Catal. Rev. (2022) 1–45.
[77] Z. Sun, T. Ma, H. Tao, Q. Fan, B. Han, Fundamentals and challenges of electrochemical CO_2 reduction using two-dimensional materials, Chem 3 (2017) 560–587.
[78] C. Li, Z. Sun, X. Dong, S. Zheng, D.D. Dionysiou, Acetic acid functionalized TiO_2/kaolinite composite photocatalysts with enhanced photocatalytic performance through regulating interfacial charge transfer, J. Catal. 367 (2018) 126–138.
[79] J. Wang, L. Zhang, D. Zeng, W. Wang, R. Li, T. Jia, B. Cui, H. Chu, W. Wang, Multi-radicals mediated one-step conversion of methane to acetic acid via photocatalysis, Appl. Catal. B-Environ. 337 (2023) 122983.
[80] F.A. Qaraah, S.A. Mahyoub, A. Hezam, A. Qaraah, Q.A. Drmosh, G. Xiu, Construction of 3D flowers-like O-doped g-C3N4-[N-doped Nb2O5/C] heterostructure with direct S-scheme charge transport and highly improved visible-light-driven photocatalytic efficiency, Chinese J. Catal. 43 (2022) 2637–2651.
[81] N. Ji, J. Yin, Y. Rong, H. Li, Z. Yu, Y. Lei, S. Wang, X. Diao, More than a support: the unique role of Nb_2O_5 in supported metal catalysts for lignin hydrodeoxygenation, Catal, Sci. Technol. 12 (2022) 3751–3766.
[82] X. Jiao, Z. Hu, K. Zheng, J. Zhu, Y. Wu, X. Zhang, J. Hu, W. Yan, J. Zhu, Y. Sun, Y. Xie, Direct polyethylene photoreforming into exclusive liquid fuel over charge-asymmetrical dual sites under mild conditions, Nano Lett. 22 (2022) 10066–10072.
[83] J.B. Williamson, S.E. Lewis, R.R. Johnson Iii, I.M. Manning, F.A. Leibfarth, C–H functionalization of commodity polymers, Angew. Chem. Int. Edit. 58 (2019) 8654–8668.
[84] A.S. Goldmann, M. Glassner, A.J. Inglis, C. Barner-Kowollik, Post-functionalization of polymers via orthogonal ligation chemistry, Macromol. Rapid Comm. 34 (2013) 810–849.
[85] N.K. Boaen, M.A. Hillmyer, Post-polymerization functionalization of polyolefins, Chem. Soc. Rev. 34 (2005) 267–275.
[86] S. Gazi, M. Đokić, K.F. Chin, P.R. Ng, H.S. Soo, Visible light-driven cascade carbon-carbon bond scission for organic transformations and plastics recycling, Adv. Sci. 6 (2019) 1902020.
[87] S.E. Lewis, B.E. Wilhelmy, F.A. Leibfarth, Upcycling aromatic polymers through C-H fluoroalkylation, Chem. Sci. 10 (2019) 6270–6277.
[88] S. Moulay, Functionalized polystyrene and polystyrene-containing material platforms for various applications, Polym-Plast. Technol. 57 (2018) 1045–1092.
[89] I.M. Maafa, Pyrolysis of Polystyrene Waste: A Review, in: Polymers, 13 (2021) 225.
[90] B.T. Ho, T.K. Roberts, S. Lucas, An overview on biodegradation of polystyrene and modified polystyrene: the microbial approach, Crit. Rev. Biotechnol. 38 (2018) 308–320.
[91] S.-C. Baek, K.-W. Jun, Y.-J. Lee, J.D. Kim, D.Y. Park, K.-Y. Lee, Ru/Ni/$MgAl_2O_4$ catalysts for steam reforming of methane: effects of Ru content on self-activation property, Res. Chem. Intermediat. 38 (2012) 1225–1236.
[92] L.-B. Gao, J. Kan, Y. Fan, L.-Y. Zhang, S.-H. Liu, Z.-N. Chen, Wirelike dinuclear ruthenium complexes connected by Bis(ethynyl)oligothiophene, Inorg. Chem. 46 (2007) 5651–5664.
[93] Y. Li, J. Yang, J. Song, Design structure model and renewable energy technology for rechargeable battery towards greener and more sustainable electric vehicle, Renew. Sust. Energ. Rev. 74 (2017) 19–25.
[94] A. Geetha, C. Subramani, A comprehensive review on energy management strategies of hybrid energy storage system for electric vehicles, Int. J. Energ. Res. 41 (2017) 1817–1834.
[95] B. Dunn, H. Kamath, J.-M. Tarascon, Electrical energy storage for the grid: a battery of choices, Science 334 (2011) 928–935.
[96] M. Centeno Brito, K. Lobato, P. Nunes, F. Serra, Sustainable energy systems in an imaginary island, Renew, Sust. Energ. Rev. 37 (2014) 229–242.
[97] W. Qian, S. Xu, X. Zhang, C. Li, W. Yang, C.R. Bowen, Y. Yang, Differences and similarities of photocatalysis and electrocatalysis in two-dimensional nanomaterials: strategies traps, applications and challenges, Nano-Micro Lett. 13 (2021) 156.
[98] J.K. Pedersen, T.A.A. Batchelor, D. Yan, L.E.J. Skjegstad, J. Rossmeisl, Surface electrocatalysis on high-entropy alloys, Curr. Opin. Electroche. 26 (2021) 100651.
[99] Y. Yang, Z. Tan, J. Zhang, Electrocatalytic carbon dioxide reduction to ethylene over copper-based catalytic systems, Chem-Asian J. 17 (2022) e202200893.
[100] A. Liu, M. Gao, X. Ren, F. Meng, Y. Yang, L. Gao, Q. Yang, T. Ma, Current progress in electrocatalytic carbon dioxide reduction to fuels on heterogeneous catalysts, J. Mater. Chem. A 8 (2020) 3541–3562.
[101] T. Zhang, X. Li, J. Wang, Y. Miao, T. Wang, X. Qian, Y. Zhao, Photovoltaic-driven electrocatalytic upcycling poly(ethylene terephthalate) plastic waste coupled with hydrogen generation, J. Hazard. Mater. 450 (2023) 131054.
[102] L. Li, X. Li, Y. Sun, Y. Xie, Rational design of electrocatalytic carbon dioxide reduction for a zero-carbon network, Chem. Soc. Rev. 51 (2022) 1234–1252.
[103] X. Huang, Y.-B. Zhang, Reticular materials for electrochemical reduction of CO_2, Coordin. Chem. Rev. 427 (2021) 213564.
[104] Q. Feng, Y. Sun, X. Gu, Z. Dong, Advances of cobalt phthalocyanine in electrocatalytic CO_2 reduction to CO: a mini review, Electrocatalysis 13 (2022) 675–690.
[105] J. Wang, X. Li, T. Zhang, Y. Chen, T. Wang, Y. Zhao, Electro-reforming polyethylene terephthalate plastic to co-produce valued chemicals and green hydrogen, J. Phys. Chem. Lett. 13 (2022) 622–627.
[106] J. Wang, X. Li, M. Wang, T. Zhang, X. Chai, J. Lu, T. Wang, Y. Zhao, D. Ma, Electrocatalytic valorization of poly(ethylene terephthalate) plastic and CO2 for simultaneous production of formic acid, ACS Catal. 12 (2022) 6722–6728.
[107] R. Shi, K.-S. Liu, F. Liu, X. Yang, C.-C. Hou, Y. Chen, Electrocatalytic reforming of waste plastics into high value-added chemicals and hydrogen fuel, Chem. Commun. 57 (2021) 12595–12598.
[108] H. Zhou, Y. Ren, Z. Li, M. Xu, Y. Wang, R. Ge, X. Kong, L. Zheng, H. Duan, Electrocatalytic upcycling of polyethylene terephthalate to commodity chemicals and H2 fuel, Nat. Commun. 12 (2021) 4679.
[109] T. Ren, Z. Duan, H. Wang, H. Yu, K. Deng, Z. Wang, H. Wang, L. Wang, Y. Xu, Electrochemical co-production of ammonia and biodegradable polymer monomer glycolic acid via the co-electrolysis of nitrate wastewater and waste plastic, ACS Catal. 13 (2023) 10394–10404.
[110] T.H.T. Myren, T.A. Stinson, Z.J. Mast, C.G. Huntzinger, O.R. Luca, Chemical and electrochemical recycling of end-use poly(ethylene terephthalate) (PET) plastics in batch microwave and electrochemical reactors, Molecules 25 (2020) 2742.
[111] D.A. Bulushev, J.R.H. Ross, Towards sustainable production of formic acid, ChemSusChem 11 (2018) 821–836.
[112] Z. Ma, U. Legrand, E. Pahija, J.R. Tavares, D.C. Boffito, From CO_2 to formic acid fuel cells, Ind. Eng. Chem. Res. 60 (2021) 803–815.
[113] Z. Fang, W. Chen, Recent advances in formic acid electro-oxidation: from the fundamental mechanism to electrocatalysts, Nanoscale Adv. 3 (2021) 94–105.
[114] R. Prins, M.E. Bussell, Metal phosphides: preparation, characterization and catalytic reactivity, Catal. Lett. 142 (2012) 1413–1436.
[115] K. He, T. Tadesse Tsega, X. Liu, J. Zai, X.-H. Li, X. Liu, W. Li, N. Ali, X. Qian, Utilizing the space-charge region of the FeNi-LDH/CoP p-n Junction to promote performance in oxygen evolution electrocatalysis, Angew. Chem. Int. Edit. 58 (2019) 11903–11909.
[116] M. Volokh, G. Peng, J. Barrio, M. Shalom, Carbon nitride materials for water splitting photoelectrochemical cells, Angew. Chem. Int. Edit. 58 (2019) 6138–6151.
[117] G. Divyapriya, S. Singh, C.A. Martínez-Huitle, J. Scaria, A.V. Karim, P. V. Nidheesh, Treatment of real wastewater by photoelectrochemical methods: An overview, Chemosphere 276 (2021) 130188.
[118] M. Ahmed, I. Dincer, A review on photoelectrochemical hydrogen production systems: challenges and future directions, Int. J. Hydrogen Energ. 44 (2019) 2474–2507.
[119] L. Hahn, B. Buttlar, E. Walther, Unpacking plastic: investigating plastic related ambivalence, Sustainability 13 (2021) 2186.
[120] S. Bhattacharjee, V. Andrei, C. Pornrungroj, M. Rahaman, C.M. Pichler, E. Reisner, Reforming of soluble biomass and plastic derived waste using a bias-free Cu30Pd70|perovskite|pt photoelectrochemical device, Adv. Funct. Mater. 32 (2022) 2109313.
[121] C.-Y. Lin, S.-C. Huang, Y.-G. Lin, L.-C. Hsu, C.-T. Yi, Electrosynthesized Ni-P nanospheres with high activity and selectivity towards photoelectrochemical plastics reforming, Appl. Catal. B-Environ. 296 (2021) 120351.
[122] U. Bassey, K. Sarquah, M. Hartmann, A.-O. Tom, G. Beck, E. Antwi, S. Narra, M. Nelles, Thermal treatment options for single-use, multilayered and composite waste plastics in Africa, Energy 270 (2023) 126872.
[123] Z. Jin, L. Yin, D. Chen, Y. Jia, J. Yuan, Y. Hu, Co-pyrolysis characteristics of typical components of waste plastics in a falling film pyrolysis reactor, Chinese, J Chem. Eng. 26 (2018) 2176–2184.
[124] F.J. Christopher, P. Senthil Kumar, L. Jayaraman, G. Rangasamy, Assessment of product distribution of plastic waste from catalytic pyrolysis process, Fuel 332 (2023) 126168.
[125] D. Yuan, X. Shen, L. Tian, D. Gu, L. Zhu, B. Wang, Solar STEP organic decomposition plus hydrogen: a novel approach to efficient degradation of organic pollutants exemplified by acrylonitrile, Int. J. Hydrogen Energ. 41 (2016) 17199–17207.
[126] C. Yan, J. Wang, H. Du, L. Zhu, T. Jiang, H. Jiang, H. Wu, B. Wang, Solar Thermal Electrochemical Process (STEP) action to biomass: solar thermo-coupled electrochemical synergy for efficient breaking of biomass to biofuels and hydrogen, Energ. Convers Manage. 180 (2019) 1247–1259.
[127] D. Yuan, S. Liu, H. Wu, D. Ji, L. Zhu, C. Nie, X. Shen, B. Wang, Three-field synergy of solar energy for induced the enhancement of the oxidation of acrylonitrile in coordination with the production of hydrogen, Int. J. Hydrogen Energ. 44 (2019) 5303–5313.

[128] S. Licht, B. Wang, S. Ghosh, H. Ayub, D. Jiang, J. Ganley, A new solar carbon capture process: solar thermal electrochemical photo (STEP) carbon capture, J. Phys. Chem. Lett. 1 (2010) 2363–2368.
[129] Z. Li, X. Xu, X. Sheng, P. Lin, J. Tang, L. Pan, Y.V. Kaneti, T. Yang, Y. Yamauchi, Solar-powered sustainable water production: state-of-the-art technologies for sunlight–energy–water nexus, ACS Nano 15 (2021) 12535–12566.
[130] W. Ding, A. Bonk, T. Bauer, Corrosion behavior of metallic alloys in molten chloride salts for thermal energy storage in concentrated solar power plants: a review, Front. Chem. Sci. Eng. 12 (2018) 564–576.